Nanoscale

REVIEW

View Article Online
View Journal | View Issue

Cite this: *Nanoscale*, 2014, **6**, 12250

Two-dimensional heterostructures: fabrication, characterization, and application

Hong Wang,[a] Fucai Liu,[a] Wei Fu,[a] Zheyu Fang,[b,c,d] Wu Zhou[e] and Zheng Liu*[a,f,g]

Received 20th June 2014,
Accepted 11th August 2014

DOI: 10.1039/c4nr03435j

www.rsc.org/nanoscale

Two-dimensional (2D) materials such as graphene, hexagonal boron nitrides (hBN), and transition metal dichalcogenides (TMDs, *e.g.*, MoS_2) have attracted considerable attention in the past few years because of their novel properties and versatile potential applications. These 2D layers can be integrated into a monolayer (lateral 2D heterostructure) or a multilayer stack (vertical 2D heterostructure). The resulting artificial 2D structures provide access to new properties and applications beyond their component 2D atomic crystals and hence, they are emerging as a new exciting field of research. In this article, we review recent progress on the fabrication, characterization, and applications of various 2D heterostructures.

1. Introduction

Materials behave significantly distinct in reduced dimensions when compared with their bulk counterparts, as exemplified by the form transition from bulk graphite to two-dimensional (2D) graphene and one-dimensional (1D) carbon nanotube. Such low dimensional crystals trigger great interest from both the fundamental and application points of view, especially for 2D graphene and graphene analogues over the last decade. In fact, the thermal stability of a single-atom-thickness sheet was studied as long ago as the late 1930s. Theorists predicted that, at room temperature, the physical reality of free-standing graphene was impossible due to the minimization of its surface energy.[1,2] Such speculation has been disproved by an experiment in 2004 when monolayer graphite was successfully isolated by Geim *et al*. on silica *via* mechanical exfoliation.[3] Since then, great attention has been paid to the 2D research field, and as a result, lots of other atomically thin 2D materials, such as hBN and MoS_2, with properties distinct from that of graphene have been prepared experimentally. Now we have 2D semimetals, semiconductors, and insulators, *etc*. These 2D members can be stacked or stitched together to form atomically thin 2D heterostructures. In 2010, Dean *et al*. introduced the first atomically thin 2D heterostructures, in which graphene was placed on top of thin hBN layers. They demonstrated that hBN can serve as an excellent 2D substrate for graphene.[4] Atomically thin 2D heterostructures have received extensive attention since then and many exciting experimental results have been reported during the past few years.[5–12]

There have appeared many reviews on 2D materials beyond graphene over the past few years;[13–18] however, 2D heterostructures have rarely been involved.[12,19] In 2013, Geim *et al*. explained the significance of 2D heterostructures and proposed some possible directions in this area.[12] In the present article, we focus on the fabrication, characterization, and applications of various 2D heterostructures.

With the upholding by van der Waals forces, it is expected that one can stack arbitrary stable 2D layers together by the exfoliation-transfer technique, but for the lateral structures fabrication, things become more complicated as atoms from different 2D materials need to bond together to form a well-stitched lateral junction. Experimentally, some typical lateral junctions, *e.g.*, graphene and hBN, have been achieved by a vapor-phase growth method. In this review, after a brief introduction of pristine 2D materials synthesis, we discuss the fabrication techniques (emphasizing the vapor-phase growth and sequential transfer methods), and the morphologies and structures of 2D heterostructures, and, where possible, the relationship between the structure and electronic properties will also be reviewed. In the last part, we summarize recent progress in electronic and optoelectronic applications of 2D heterostructures.

[a]*School of Materials Science and Engineering, Nanyang Technological University, Singapore 639798. E-mail: z.liu@ntu.edu.sg*
[b]*School of Physics, State Key Lab for Mesoscopic Physics, Peking University, Beijing 100871, China*
[c]*Collaborative Innovation Center of Quantum Matter, Beijing 100871, China*
[d]*Department of Electrical and Computer Engineering, and Laboratory for Nanophotonics, Rice University, 6100 Main Street, Houston, Texas 77005, USA*
[e]*Materials Science & Technology Division, Oak Ridge National Lab, Oak Ridge, TN 37831, USA*
[f]*NOVITAS, Nanoelectronics Centre of Excellence, School of Electrical and Electronic Engineering, Nanyang Technological University, Singapore 639798*
[g]*CINTRA CNRS/NTU/THALES, UMI 3288, Research Techno Plaza, 50 Nanyang Drive, Border X Block, Level 6, Singapore 637553*

2. Pristine 2D materials synthesis

This review mainly deals with the 2D materials based heterostructures. As is well known, vapor-phase growth and the sequential transfer method have been recognized as two of the most effective ways to obtain 2D heterostructures. The vapor-phase growth of 2D heterostructures has much in common with pristine 2D materials growth. Therefore, before discussing 2D heterostructures fabrication, we will give a short review of the synthesis of pristine 2D materials, with an emphasis on the vapor-phase growth method.

Graphene Atomically thin graphene was first prepared by Geim *et al*. *via* a mechanical exfoliation method.[3] Such graphene has a very high-quality, yet the method has a poor output. In order to scale up the applications of graphene, there is a great need to develop a neat and inexpensive method for the synthesis of large-area and high-quality graphene in great uniformity and continuity. Silicon carbide (SiC) was found to be an excellent substrate for the epitaxial growth of wafer-size graphene in 2004.[20] Since then, significant advances have been made in this area. The quality of graphene has thus considerably improved in recent years.[21–25] The possibility of large integrated electronics on SiC-epitaxial graphene was also first proposed around the same time. Hundreds of transistors on a single chip[26] were made by MIT researchers in 2009, with very high frequency transistors produced on monolayer graphene on SiC.[27] Alternatively, a large variety of metals (Ni,[28–38] Cu,[37,39–44] Pt,[45–48] Co,[37,49,50] Ru,[51,52] Ir,[53,54] Pd,[55] Ag,[56] Au,[57] Ga,[58–60] Ge,[61,62] Mo,[63,64] W,[64] Ti,[64] Zr,[64] Hf,[64] V,[64] Nb,[64] Ta,[64] and In[65]) and alloys (Cu–Ni,[66,67] Cu–Co,[68] Cu–Ag,[69] Ni–Mo,[70] Ni–Ge,[71] Ni–Au[72]) have been demonstrated for the growth of graphene *via* a surface reaction process or the surface segregation of carbon upon cooling from a metastable carbon–metal solid solution using a CVD method (summarized in Table 1). The carbon solubility in the metals and the growth conditions determine the deposition mechanism, which ultimately also defines the morphology and thickness of the graphene films.[73] Specifically, Ni and Cu have been found to be excellent substrates for growing large-scale and high-quality graphene in a low-cost and controlled way.[28,44] To date, single-crystal graphene up to a centimeter and wafer size[61,74–78] and polycrystalline graphene up to forty inches size[79,80] can be grown by an optimized CVD process.

hBN Hexagonal boron nitride (hBN) is a common nontoxic material, used for its excellent electrical insulation, high thermal conductivity, and superior lubricant properties. hBN atomic layers are an important complementary 2D crystal and substrate to graphene because their atomically smooth surface and strong ionic bonding significantly reduce the charge traps on the surface,[81] and thus improve the carrier mobility of graphene by about one order higher than SiO_2 substrates.[4,82] Like graphene, micromechanical cleavage can be employed to prepare atomically thin hBN from its bulk counterpart. However, the small size (a few microns and even less) and extremely low output of the resulting hBN flakes limit its applications.

Pioneering work on the synthesis of hexagonal boron nitride atomic layers by a CVD process has been reported over the past few years. Song *et al*. demonstrated the large-scale growth of hBN layers *via* a low-pressure assisted CVD (LPCVD) method, using ammonia borane (NH_3-BH_3) as the sources of B and N and Cu as the substrate.[83,84] A few months later, Shi *et al*. reported a similar approach using borazine ($B_3N_3H_6$) as the source and Ni as the substrate.[85] Other compounds, such as trichloroborazine ($B_3N_3H_3Cl_3$) and hexachloroborazine ($B_3N_3Cl_6$), were also used *via* pyrolysis to form hBN thin films.[86] Recently, large-area uniform monolayer hBN was obtained on Cu[87,88] and Pt[89] foils *via* a LPCVD method. Single-crystal monolayer hBN up to several microns has also been synthesized on electropolished or pre-annealed Cu foils.[90,91]

TMDs Transition metal dichalcogenides (TMDs) are a diverse and large class of layered materials, consisting of more than 40 members which possess a variety of physical properties.[101–103] Molybdenum disulfide (MoS_2), as a representative of the TMD family, has recently attracted tremendous attention as a channel material for field-effect transistors.[104] With a large "ON/OFF" ratio and reasonable charge carrier mobility, this material may be a good candidate for application in semiconducting technologies. Developments in the vapor-phase growth of TMDs can be primarily divided into solid state sulfurization of the transition metal containing films[105] and chemical vapor growth through the reaction of sulfur and transition metal oxides.[106,107] In the case of MoS_2 thin films, an easy approach was first developed by sulfurizing molybdenum films in order to prepare MoS_2.[105] In addition to silica, monolayer and high-quality MoS_2 was also grown on nearly lattice-matching mica substrates, and the growth was proposed to follow an epitaxial growth mechanism.[108] With various aromatic molecules as growth seeds, large-area uniform monolayer MoS_2 was synthesized on diverse substrates.[109,110] So far,

Table 1 A summary of the elements and alloys used as substrates for the CVD growth of graphene. Blue shading refers to substrates suitable for a few-layer graphene growth. Pink shading indicates polycrystalline substrates that can be used for growing highly uniform monolayer (>95% coverage) graphene under optimized CVD conditions. Single-crystal substrates that support the growth of uniform monolayer graphene are shaded green. White shading indicates the substrates on which there is no report of graphene yield

									Al	Si
Ti	V	Cr	Mn	Fe	Co	Ni	Cu	Zn	Ga	Ge
Zr	Nb	Mo	Tc	Ru	Rh	Pd	Ag	Cd	In	Sn
Hf	Ta	W	Re	Os	Ir	Pt	Au	Hg	Tl	Pb

Cu-Ni	Cu-Co	Cu-Ag
Ni-Mo	Ni-Ge	Ni-Au

Table 2 Experimental results on some 2D monolayers grown from the vapor phase

Monolayers	Band gap (eV)	Max polycrystalline film size	Max single crystal size	Max mobility on SiO_2/Si ($cm^2 V^{-1} s^{-1}$)
Graphene	0	40 inches[80]	5.08 cm[61]	16 000[77]
hBN	~6.0	7 cm × 7 cm[88]	~10 μm[90,91]	—
MoS_2	~1.8	1 cm × 3 cm[92]	~123 μm[93]	7[94]
WS_2	~2.1	1 cm × 1 cm[95]	~180 μm[96]	0.46[97]
$MoSe_2$	~1.5	1.5 cm × 2 cm[98]	~135 μm[99]	50[99]
WSe_2	~1.7	~1 inch[100]	~50 μm[100]	90[100]

high-quality and single-crystal MoS_2 layers can be synthesized *via* various methods and have been comprehensively characterized in terms of atomic structures, electronic transportation, and electronic logic devices. The preparation of wafer-size continuous MoS_2 films and large single-crystal domains is an ongoing challenge. Besides MoS_2, many other layered sulfides and selenides, such as WS_2,[96,97,111] $MoSe_2$,[99,112] and WSe_2,[100] were also prepared by a similar vapor-phase growth method. We note that, compared to the surface reaction growth of graphene and hBN, the vapor-phase growth of TMDs is less controlled and has poor repeatability. In Table 2, we summarize the progress on pristine 2D materials growth from the vapor phase, including the maximum polycrystalline film and single crystal size, and the maximum mobility (on SiO_2/Si) that have been achieved so far.

3. Fabrication and structural characterization of 2D heterostructures

3.1. Lateral heterostructures

"Lateral heterostructure" refers to a material system that consists of different 2D crystals bonded in a single atomic layer; it is an extension of the conventional "heterostructure" concept into the 2D regime. Modification of the pristine 2D materials fabrication technique allows us to obtain different 2D layers in one plane. Due to their relatively small lattice mismatch (1.7%) and the same crystal structure, graphene and hBN were considered to be integrated into a single atomic layer. The electronic band structures and properties of these lateral graphene-hBN (G-hBN) heterostructures were expected to be different from that of pristine graphene and hBN,[113–115] giving rise to the potential for the development of band-gap-engineered applications in electronics and optoelectronics.[116] Experimentally, it has been demonstrated that the shape-controlled lateral heterostructures could find applications in 2D electronic devices, such as p–n junctions, atomically thin integrated circuitry, and in split closed-loop resonators.[117,118]

3.1.1. Lateral G-hBN heterostructures with randomly distributed domains. As discussed earlier, high-quality graphene and hBN can both be synthesized on metal substrates (Cu, Ni, *et al.*) by CVD with different precursors. It is reasonable then that one can modify the growth process to deposit graphene and hBN domains in one plane. Fig. 1a is an illustration of a two-step growth method: hBN (graphene) domains were firstly grown on metal substrates, followed by the growth of graphene (hBN) domains on the uncovered metal surfaces. With this procedure, graphene and hBN lateral heterostructures can be created on various metal single crystals under UHV (Fig. 1b).[119] These samples are suitable for atomic scale characterization of the interface structures, but are not feasible for scalable fabrication. CVD on poly-crystalline Cu was used as a simple way to realize the G-hBN lateral heterostructures.[117,118,120,121] Miyata *et al.* found that during the two-step deposition of graphene and hBN on Cu foils, the hBN growth was initiated preferentially at the edge of the graphene grains (Fig. 1c).[122]

In addition, the one-step growth method may also lead to lateral heterostructures. Fig. 1d shows an experimental configuration for preparing such lateral G-hBN heterostructures.[114] At ~1000 °C temperature, CH_4 as the C source and NH_3-BH_3 as the B and N sources were simultaneously introduced into the furnace to support the growth of G-hBN heterostructures on Cu foils. Fig. 1e shows an AFM image of the resulting hybrid film. Based on the experimental results and theoretical calculations, Ci *et al.* believed that the hybrid hBNC films (BN concentrations >10%) consisted of randomly distributed domains of nanometer-sized graphene and hBN connected in one plane, forming a large number of lateral heterostructures. By adjusting the partial pressure of CH_4 and NH_3-BH_3, they could tune the BN concentrations in the hBNC films, and therefore modify the properties of the hBNC films.[123] Liu *et al.* further demonstrated that by optimizing the growth conditions, the graphene and hBN domain size in the hBNC films could be increased to a few hundreds of microns.[118]

Chang *et al.* performed experimental investigations of the phase separation and band structure of hBNC films at low BN concentrations.[114] The BN content in the graphene layers was tuned by changing the heating temperature of the NH_3-BH_3 precursor, and was further confirmed by X-ray photoelectron spectroscopy (XPS). The structural evolution of the hBNC film with different BN concentrations was characterized using TEM. As shown from Fig. 2a–2c, no BN phase was observed in 2BNG (2% BN-doped graphene) film, and the segregation of the BN domains is found to occur for BN concentration above 8%. Fig. 2d is an illustration of the structural evolution in hBNC films with different BN concentrations. Such a structural evolution has a significant influence on the electronic structure of hBNC films, as confirmed by the X-ray absorption (XAS) and emission (XES) spectroscopy measurements. Fig. 2e shows the C K-edge XAS and K_α XES spectra of pristine graphene and hBNC samples. We note that the band gap increases with the BN concentrations, reaching 600 meV for the 6% BN-doped sample. Further increases of the BN concentration will lead to a decrease in the band gap. For a BN concentration of 52%, no band gap is observed, which is similar to the pristine graphene situation.[114] The band gap opening in BN-doped graphene was

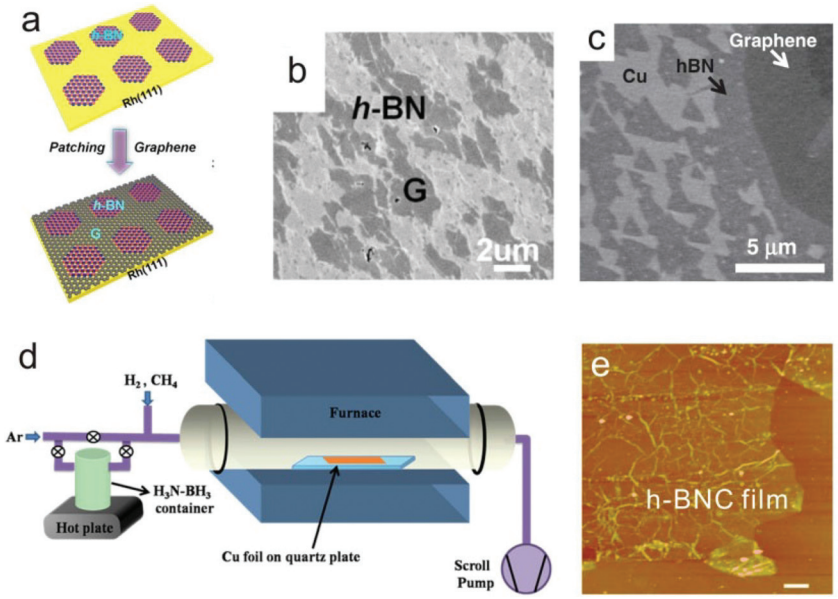

Fig. 1 Synthesis and characterizations of lateral G-hBN heterostructures with randomly distributed domains. (a) A schematic of the two-step growth procedure. (b) SEM image of lateral G-hBN heterostructures grown on a Rh(111) substrate.[119] (c) SEM image showing the higher density of hBN nucleation at the edge of a graphene grain.[122] (d) A schematic of the CVD setup for growing G-hBN heterostructures.[114] (e) An AFM image showing hBNC film with a uniform thickness (scale bar: 1 μm).[123] Reprinted with permission from: (a, b), ref. 119, © 2013 ACS; (c), ref. 122, © 2012 The Japan Society of Applied Physics; (d), ref. 114, © 2013 ACS; (e), ref. 123, © 2010 NPG.

attributed to the breaking of the carbon sublattice symmetry.[124] We also note another experimental report about the band gap opening in the hBNC film, which was made by Ci *et al*. Using temperature-dependent resistance measurements, they revealed a ~18 meV band gap in hBNC film with a 56% carbon content (Fig. 2f), and attributed it to the quantum confinement and/or spin polarization at specific C–BN boundaries.[123] These experimental results confirm that the electronic structure of hBNC varies depending on the stoichiometry of carbon and BN.

3.1.2. Shape-controlled lateral G-hBN heterostructures. Although lateral G-hBN heterostructures have been theoretically and experimentally investigated,[117,125] the fabrication of heterostructures with the size and shape of different domains engineered precisely for novel electronic devices has been scarcely realized. Gong *et al*. developed a novel method to construct shape-controlled lateral heterostructures.[126] As shown in Fig. 3a, they first transferred CVD-graphene to a Si substrate, then a 50 nm thick SiO_2 layer with predefined patterns was deposited on top of the graphene, and then the whole chip was loaded into a CVD furnace to convert the uncovered graphene to hBN or hBNC, with boric acid as the B source and ammonia as the N source. When the SiO_2 mask was removed, they obtained lateral G-hBN heterostructures. This method relies on the ability to chemically convert graphene to hBN at high temperatures with foreign B and N sources. Furthermore, if the conversion reaction time is less than 2 h, graphene will be partially converted to hBNC. Therefore, G-hBNC–hBN lateral structures can also be fabricated with a two-step conversion process.[126]

In addition, Levendorf *et al*. and Liu *et al*. developed a two-step, scalable approach to create planar G-hBN structures,[117,118] in which periodic arrangements of domains with sizes ranging from tens of nanometers to millimeters were created. The approach started with the CVD growth of hBN on Cu/Ni foils; then the as-prepared hBN was lithographically patterned, and finally graphene was grown in the patterned hBN atomic layers (Fig. 3b). *Via* this approach, the controlled size and shape of different domains were achieved and sharp G-hBN interfaces could be created, *e.g.*, G-hBN rings (Fig. 3d), G-hBN squares, and G-hBN stripes.[118] TEM imaging and elemental analysis show that the interface between graphene and hBN are contiguous. The width of the interface is less than 1 nm. However, it is still a challenge to get atomic resolution images of the interface by annular dark field scanning transmission electron microscopy (ADF-STEM) due to the polymer contamination on the surface. The seamless integration of graphene and hBN makes it possible to fabricate complicated hybridized structures, where hBN can serve as an insulating dielectric matrix for graphene and as an important complementary component. For instance, a G-hBN split closed-loop resonator[127] is directly grown using a similar CVD approach as discussed above. This split closed-loop resonator generates a resonating frequency at ~1.9 GHz, a value close to the value of copper strip based on similar geometries.[128] Levendorf *et al*. fabricated perfectly flat lateral junctions between electrically conductive graphene and insulating hBN (Fig. 3e). They demonstrated that such a structure could be used for producing atomically thin integrated circuits.[117] These results suggest that lateral G-hBN films

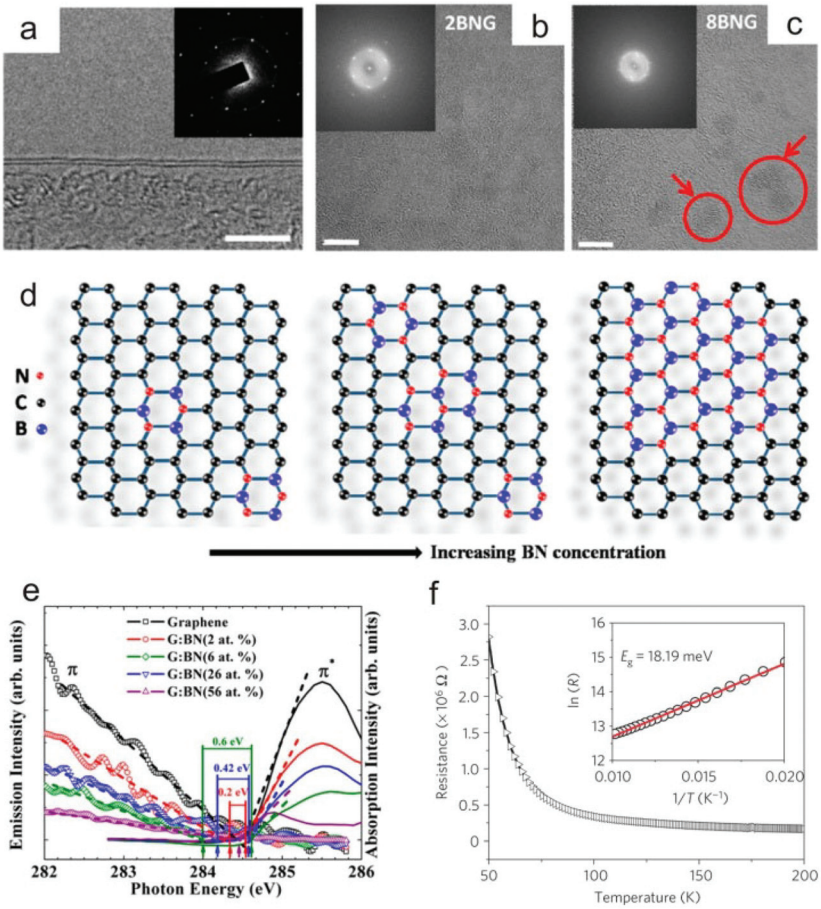

Fig. 2 Structural evolution and band gap opening in hBNC films. (a) High-resolution TEM image of a hBNC film showing the layer number. Inset is the electron diffraction pattern taken at the corresponding region. (b) High-resolution TEM image of 2BNG (2% BN-doped graphene) sample. Inset is the corresponding fast-Fourier transform (FFT), showing only the graphene crystalline structure. (c) High-resolution TEM image of 8BNG sample depicting the distribution of hBN domains (encircled regions) in graphene. The inset is the FFT of the image, indicating the presence of the crystalline domains of both graphene and hBN. (Scale bar is 5 nm). (d) Schematic diagram depicting the structural evolution in BNG films with the increase in BN concentration. (e) Normalized C K-edge XANES and Kα XES spectra at the π–π* region of the BNG films. (f) A resistance-*versus*-temperature curve for a hBNC film. The inset shows ln(R) as a function of T^{-1} in the temperature range from 50 to 100 K. The linear fit (solid line) shows that the data are well described by $R(T) \propto \exp(E_\Delta/k_B T)$. E_Δ is the band gap and k_B is Boltzmann's constant. Reprinted with permission from: (a–e), ref. 114, © 2013 ACS; (f), ref. 123, © 2010 NPG.

can be grown directly by CVD, thus providing opportunities for the fabrication of various novel devices, although further efforts are required to optimize their performances.

3.1.3. Interface structure of G-hBN lateral heterostructures. For the characterization of lateral heterostructures, there are two fundamental issues to be addressed. The first is whether an epitaxial structural relationship can exist between the components. The other is how the different atoms bond at the interfaces. Scanning tunneling microscopy (STM) is a powerful tool for investigating the atomic scale information at the interface of lateral heterostructures. Significant progress has been made in the STM characterization of lateral G-hBN junctions.[119,121,129] Fig. 4a shows G-BN heterostructures on Ru(0001), the growth was performed in UHV by consecutive exposure of Ru(0001) single crystals to ethylene and borazine at high temperatures. Moiré structures of monolayer graphene and hBN on Ru(0001) feature differently in the STM images (Fig. 4a), which makes it possible to distinguish the monolayer graphene and hBN areas. Though the graphene moiré structure terminates in an atomically sharp edge, there is an interfacial zone to connect hBN with graphene, which display as faint lines (L) and atomic-scale point-like protrusions (Fig. 4b). The atomic-scale investigation suggests that the interfacial zone is a substitutional B–C–N phase, which forms in the beginning of the BN growth process due to the incorporation of C from the metal surface into the growing hBN. By using an additional well-controlled O_2 etch process to etch C adatoms and possibly some of the graphene edge before the BN growth, they obtained G-BN heterostructures with atomically sharp interfaces, as shown by the high resolution STM image (Fig. 4c).[129] This study provides insight into the influence of growth conditions on interfacial structures of 2D lateral junctions.

Due to graphene and hBN both being epitaxially grown on the same single-crystal substrate, it is reasonable to assume

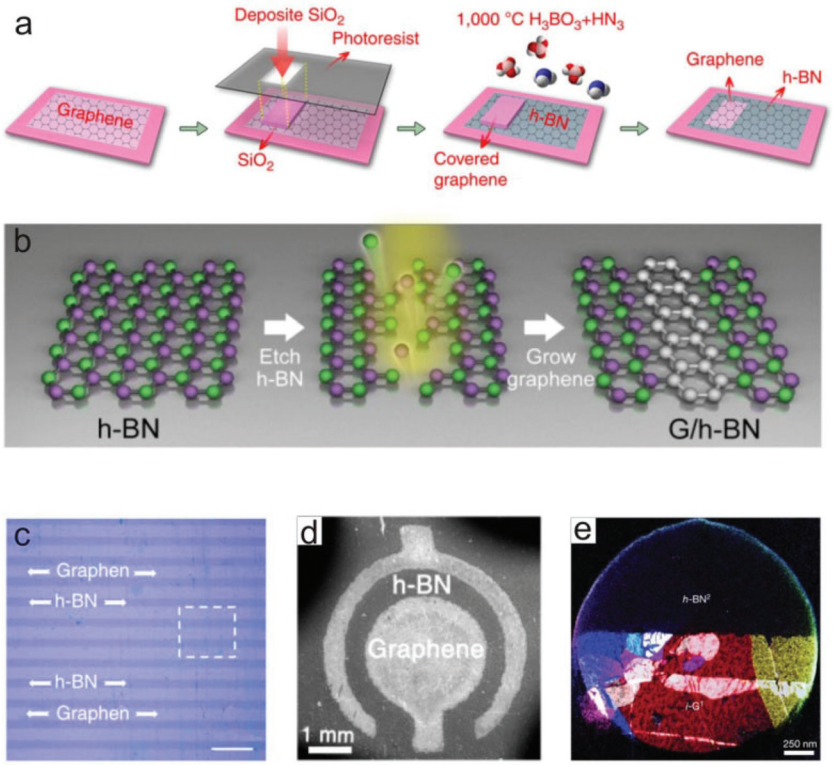

Fig. 3 Shape-controlled lateral G-hBN heterostructures fabrications. Schematics of the fabrication procedures for lateral G-hBN heterostructures by: (a) a spatially controlled conversion process,[126] and (b) a two-step growth process.[118] (c) Optical image of G-hBN strips on a SiO_2 substrate fabricated by the method illustrated in (a), scale bar: 10 μm. (d) SEM image showing G-hBN rings fabricated by the method illustrated in (b). (e) False-color dark-field TEM image showing a suspended G-hBN junction. Reprinted with permission from: (a, c), ref. 126, © 2014 NPG; (b, d), ref. 118, © 2013 NPG; (e), ref. 117 © 2012 NPG.

that they have the same lattice orientation. However, it remained unclear whether such an in-plane epitaxial relationship of graphene and hBN can be realized on a polycrystalline substrate. As we mentioned earlier, lateral G-BN heterostructures have been successfully grown on Cu foil substrates by several groups,[117,118,120] but the interface structures were rarely investigated, possibly due to contaminations on the G-hBN surface during sample preparation. Liu *et al.* demonstrated the heteroepitaxial growth of lateral graphene and hBN junctions on polycrystalline Cu foils. They first performed a H_2 etch process to obtain a fresh edge of graphene grown on Cu, then monolayer hBN was grown from the fresh edges of graphene with NH_3-BH_3 as the source (Fig. 4d).[121] Fig. 4e shows the STM image of the boundary of lateral G-hBN heterostructures grown on Cu; graphene and hBN regions can be differentiated by their distinct scanning tunneling spectra (STS: dI/dV *vs.* V spectra) (Fig. 4f). We note a seamless connection of graphene and hBN at the boundary (zigzag orientation), indicating a high-quality heteroepitaxial growth. Furthermore, Liu *et al.* also demonstrated that under a low growth rate, the hBN lattice orientation is solely determined by the graphene seed, independent of the underlying Cu lattice.[121]

To summarize, G-hBN lateral structures have been successfully created and extensively investigated. It should be noted that TMD materials with a similar lattice structure are ideal candidates for the construction of lateral heterostructures, because of the similar structures and many vibrations in the TMD 2D materials. For example, it is expected that the MoS_2/WS_2, MoS_2/$MoSe_2$, or similar TMD heterostructures can be synthesized using the vapor-phase growth method. Considering that many TMDs are semiconductors with different band gaps, it would be quite interesting to study the transport and light emitting properties along their interfaces. Very recently, it has been demonstrated that monolayer lateral heterostructures composed by $MoSe_2$ and WSe_2, can be synthesized *via* a simple physical vapor transport method.[130] This study will lead to the exploration of semiconducting heterostructures within a single atomic layer.

3.2. Vertical heterostructures

Layered crystals are characterized by strong intralayer covalent bonding and relatively weak interlayer van der Waals bonding. Since various methods have been proposed to make atomic layered 2D materials, such as graphene, hBN, TMDs, and oxides, it becomes possible to pick, place, and stack atomic layers of arbitrary compositions and thus to build unique artificial architectures techniques with desired functionalities.

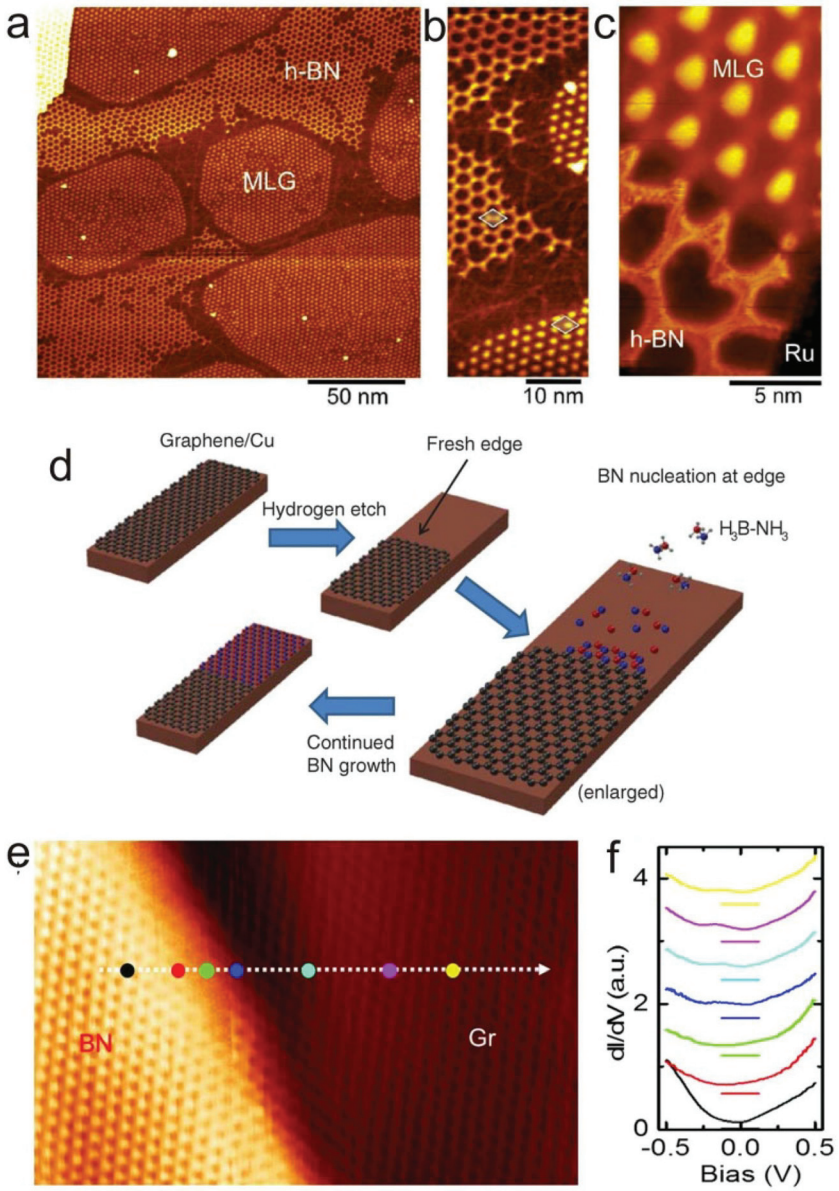

Fig. 4 STM characterization of lateral G-hBN junctions. (a–c) G-hBN heterostructure grown on Ru(0001).[129] (a) Low-magnification STM image showing no characteristic moiré structure near the interfaces of pure graphene and hBN. (b) High-magnification image of the G-hBN boundary. (c) High-resolution STM image showing atomically sharp G-hBN interface formation by sequential graphene growth, oxygen etching of C adatoms, and hBN growth.[129] (d) Illustration of lateral G-hBN heterostructures grown on Cu foils. The process involves hydrogen etching of the graphene edge before hBN growth.[121] (e) STM image (8 nm by 5 nm) of a G-hBN boundary, with colored dots marking the locations of the STS acquisition. (f) d*I*/d*V* curves color coded by location and offset for clarity, with horizontal lines indicating zero differential conductance.[121] Reprinted with permission from: (a–c), ref. 129, © 2013 ACS; (d–f), ref. 121, © 2014 AAAS.

A large number of vertical heterostructures, including G/hBN (Graphene on hBN) stack, hBN/G (hBN on Graphene) stack, G/TMD stack, TMD/TMD stack, and G/hBN superlattice, have been investigated in experiment and in theory, and some of them show great potential for applications in electronics, optoelectronics, *etc*. The creation of artificial 2D layers *via* combinatorial technologies has been proposed, where the manipulation, transfer, and stacking of isolated, mechanical exfoliated 2D layers could be employed to create high-quality stacking. This multi-step growth can be used to sequentially synthesize different layers on proper substrates for scalable 2D stacks. Liquid exfoliation and assembling can be employed to produce massive 2D layers and will be applicable to most 2D materials. The overall composition of these solids can be controlled by varying the initial concentration of the mixture. As a novel approach, mixing exfoliated atomic layers of various compositions will produce random layer stacks and could lead to enormous possibilities for new types of stacked layers. In addition, the stacking layers could be also created by heteroepitaxial growth, even with a large lattice mismatch between the grown and the substrate materials.

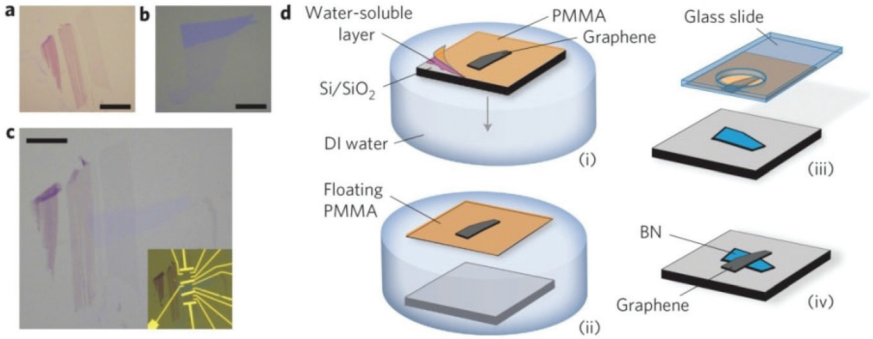

Fig. 5 Vertical G/hBN heterostructures fabricated by the transfer process. (a–c) Optical images of graphene (a) and hBN (b) before and after (c) transfer. Scale bars, 10 μm. (d) Schematic illustration of the transfer process used to fabricate graphene-on-BN devices. Reprinted with permission from ref. 4, © 2010 NPG.

3.2.1. Graphene and hBN (G-hBN) stacks. The successful preparation of atomically thin 2D materials makes it possible to stack them together to form vertical heterostructures. G/hBN and hBN/G stacks are the first demonstrated examples of this kind of 2D heterostructures.

Transfer method. Mechanical exfoliation allows the preparation of a large variety of 2D layers on a substrate, thus one can pick these 2D flakes and stack them to form vertical heterostructures. In 2010, Dean *et al*. developed a transfer technique to obtain high-quality G/hBN stacks,[4] as shown in Fig. 5d. The key idea of this method is to use a micromanipulator to precisely place graphene closely aligned to the BN flakes under an optical microscope, then the two different layers are attached closely by van der Waals forces. Fig. 5a–c show the optical images of graphene, hBN, and the resulting G/hBN stack on 285 nm SiO_2/Si substrates. Electronic transport measurements on the graphene on the hBN device show a high carrier mobility up to 60 000 $cm^2\ V^{-1}\ s^{-1}$, indicating that hBN serves as a perfect substrate for graphene electronics.[4] This method has provided a strong impetus for many subsequent research investigations into the properties and applications of vertical 2D heterostructures. Additionally, we also note that other modified transfer techniques have been developed in the last few years.[131–134]

hBN has an atomic-level smooth surface that can suppress rippling in graphene. Xue and Decker *et al*. investigated the topography and local electronic structure of graphene on hBN substrates using STM, respectively.[81,135] As shown in Fig. 6a, the roughness of graphene on hBN is greatly decreased compared to that of graphene on SiO_2 substrates. Furthermore, it was also demonstrated that the charge density inhomogeneity in graphene on hBN was significantly reduced compared to that of graphene on SiO_2. Therefore, the low density regime and the Dirac point can be more readily accessed for graphene on hBN substrates, allowing an investigation of the intrinsic transport properties of graphene.

As we already know, the interface is critically important to the performance of a heterostructure device. High-resolution STEM can provide us a cross-sectional view of vertical heterostructures. During the fabrication of heterostructures by the layer by layer transfer method, absorbates such as hydrocarbons tend to get absorbed and trapped between the layers, and are then observed as bubblers at the interface with SEM. The number of these bubblers can be largely reduced with

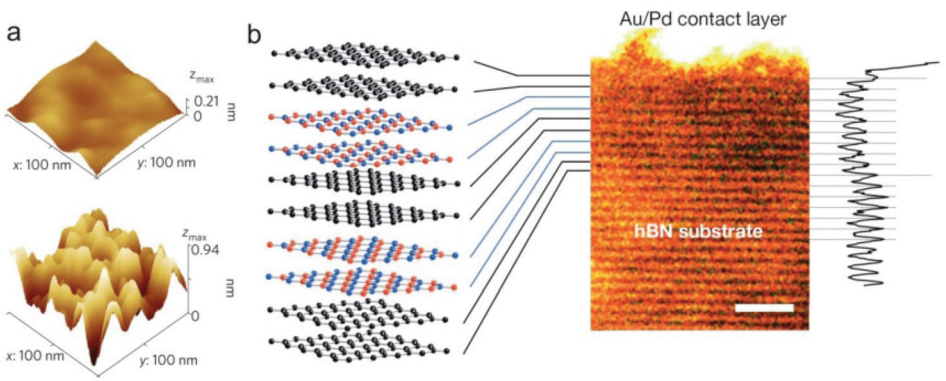

Fig. 6 Characterizations of vertical heterostructures composed of graphene and hBN. (a) STM topographic image of monolayer graphene on hBN (up) and SiO_2 (down) showing the underlying surface corrugations.[81] (b) Graphene-hBN superlattice consisting of six stacked bilayers. Right: STEM image showing the cross-section and intensity profile; Left: Schematic of the layer sequence. Scale bar, 2 nm. Reprinted with permission from: (a), ref. 81, © 2011 NPG; (b), ref. 12, © 2013 NPG and ref. 136, © 2012 NPG.

heat treatment of the heterostructures. Fig. 6b display a cross-sectional STEM of a graphene-BN superlattice, which consists of alternate graphene and hBN bilayers. The spacing between hBN and the graphene planes is found to be indistinguishable from the basal plane separation in bulk hBN, therefore, the superlattice shows an atomically sharp interface.[136] It is believed that such an atomically sharp interface can hardly be achieved *via* the direct growth method. However, as will be shown later, recently Lin *et al*. demonstrated that the vapor-phase growth of TMD layers on epitaxial graphene on 6H-SiC (0001) can also lead to atomically sharp interfaces.[137]

Synthesis methods. Though the mechanical transfer method has produced very high quality heterostructures suitable for lab research, the small sample size and poor output limit its application. Furthermore, vertical heterostructures fabricated by this method are usually randomly stacked, and particular stacking orders between different layers remain difficult to achieve. Therefore, it is highly desirable to develop a scalable method to synthesize these heterostructures.

The technique to grow high-quality pristine 2D materials by CVD can be added to the toolbox for the creation of large-area vertical heterostructures. Individual 2D layers can be grown separately, and then transferred layer by layer to form a large-area stack. Vertical heterostructures prepared by this method have found applications in large-scale 2D electronics and photoelectronics.[138,139] However, the wet transfer method that is widely used inevitably brings cracks and contaminations to the films, thus a high-quality interface of the stack cannot be expected. An alternative method is the direct growth of one kind of 2D material onto another to fabricate vertical 2D heterostructures. This method allows the realization of a clean heterostructures interface if the "as-substrate" 2D layer is free of dangling bonds.

As mentioned earlier, the CVD growth of hBN shares a lot in common with graphene. For example, copper was found to be the most suitable substrate for both of their growths. We can imagine that the two materials could be integrated into stacks with a rational design of the CVD process. There exists a lot of research on the growth of graphene and hBN stacks. The first demonstration of a large-area 2D materials stack was the fabrication of hBN on graphene (hBN/G) heterostructures.[140] Here, graphene is first grown on Cu foils, following by the growth of hBN (Fig. 7a). The size of the hBN/G stack can be up to a few centimeters. The graphene is a monolayer, while hBN

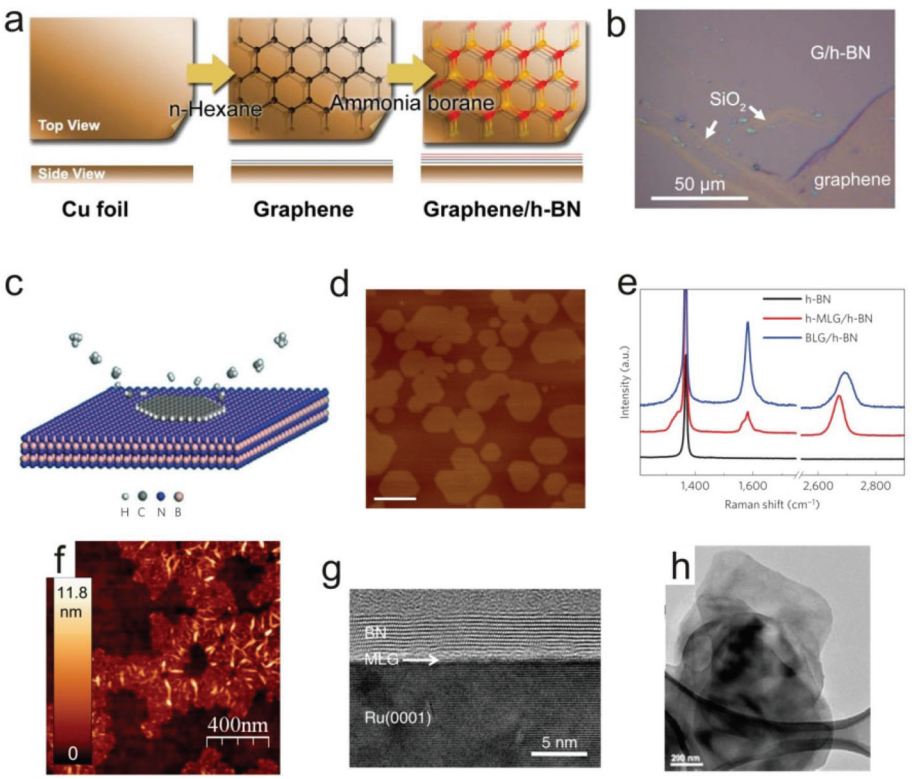

Fig. 7 Vertical graphene and hBN heterostructure synthesis. (a) Schematic of the two-step CVD synthesis of hBN on graphene: graphene was grown on Cu foils first, followed by the growth of few-layer hBN. (b) Optical image showing that the hBN on graphene films are uniform and continuous on the substrate.[140] (c–e) Graphene grains growth on exfoliated hBN flakes by PECVD. (c) is a schematic of the growth process, (d) and (e) show the AFM image and Raman spectra for the prepared graphene grains on hBN.[141] (f) 1.5 × 1.5 μm^2 AFM image showing the monolayer graphene nanodomains grown on hBN by MBE.[142] (g) HRTEM image of a 10-layer BN film grown on monolayer graphene by magnetron sputtering.[143] (h) Low-resolution TEM images of few-layer hBN/G hybrid stacking prepared by the liquid phase exfoliation-mixing method.[144] Reprinted with permission from: (a, b), ref. 140, © 2011 ACS; (c–e), ref. 141, © 2013 NPG; (f), ref. 142, © 2012 Elsevier Ltd; (g), ref. 143, © 2012 ACS; (h), ref. 144, © 2012 ACS.

is a few nanometers thick. From the optical image in Fig. 7b, we can distinguish the regions of the hBN/G stack, pure graphene, and the SiO_2 substrates by their contrast.

Encouraged by the fact that hBN can serve as an excellent dielectric substrate for graphene research, much effort has been directed toward the direct synthesis of G/hBN heterostructures. Yan *et al*. reported the growth of a large-area bilayer graphene on hBN substrate with the assistance of Ni.[145] CVD-grown hBN was transferred to a SiO_2/Si substrate, followed by spin-coating a few nm thick polymer films, and then evaporating a 500 nm Ni film on the top, after first annealing the substrate at 1000 °C with an Ar/H_2 flow and dissolving the Ni film, so that twisted bilayer graphene could be found on the hBN.[145] Son *et al*. demonstrated the metal-free growth of graphene pads on hBN layers by atmospheric chemical vapor deposition (APCVD); the graphene pads showed a thickness of ~0.5 nm and sizes up to 110 nm.[146] Wang *et al*. demonstrated the growth of a large-area G/hBN stack on a Cu substrate by a two-step CVD process.[147] The ambition of this work was to realize large-scale graphene electronics with hBN as a perfect substrate; however, the mobility of the grown graphene on hBN substrate was only of the order of 10^3, which may result from the limited quality of the grown graphene and hBN as well as their interface contamination. In spite of these achievements, however, it should be noted that in these studies, the lattice orientation relationship of graphene and hBN in the vertical stack was not investigated.

Realization of lattice alignment is an important issue for 2D stacks. As the lattice mismatch between graphene and hBN is small (1.7%), a natural question is whether an epitaxial relationship can be realized between hBN and graphene lattices. Using a plasma enhanced chemical vapor deposition (PECVD) method, Yang *et al*. reported the growth of graphene grains on hBN crystals with a fixed stacking orientation (Fig. 7c–e). The half-integer quantum Hall effect (QHE) was observed in the 2D superlattice structures, which indicated the high quality of the stack.[141] However, the size of the grown graphene grain is only hundreds of nanometers, and it is still a challenge to achieve large-area continuous G/hBN vertical heterostructures. Roth *et al*. successfully grew heterostacks consisting of monolayer graphene on hBN on a Cu(111) substrate under UHV. The lattice of graphene and hBN were well aligned in the heterostacks.[148] Tang *et al*. also demonstrated the ability to grow graphene grains on hBN crystals with a catalyst-free CVD method,[149,150] where they found that graphene aligns precisely with the underlying hBN lattice, within an error of less than 0.05°.[150] Kim *et al*. demonstrated the growth of G/hBN and hBN/G hybrid structures, using a sequential CVD growth method with Cu foil as a catalytic metal substrate. Both lateral and stacked heterostructures can be observed in the same sample. For stacked layers, turbostratic stacking and the lattice-aligned stacking of graphene and hBN were both observed, depending on the synthesis sequence.[151]

Although much effort has been directed toward the CVD synthesis of G/hBN stacks, the quality of G/hBN is still far from that of the exfoliated samples. Also, the layer number control of the G/hBN heterostructures is another issue that has not been well addressed.

In addition to the above synthetic techniques, other approaches have also been proposed for the preparation of vertical G/hBN heterostructures. Garcia *et al*. demonstrated the molecular beam epitaxy (MBE) growth of graphene on exfoliated hBN flakes, but the graphene domains are limited to the nanometer size (Fig. 7f).[142] Lin *et al*. reported a hydrogen flame method to prepare graphene on hBN flakes with PMMA as the carbon source.[152] Lin *et al*. demonstrated that a microwave method can be used for the fabrication of graphene on hBN crystals.[153] Sutter *et al*. demonstrated the synthesis of high-quality few-layer BN with a uniform thickness on a monolayer graphene covered Ru(0001) substrate by the magnetron sputtering of B in N_2/Ar (Fig. 7g).[143] A liquid-phase method was also successfully applied for the preparation of stacked atomic layers. Gao *et al*. reported that randomly stacked layers of graphene and hBN can be obtained by a chemical exfoliation-mixing method (Fig. 7h). Hybrid G/hBN films with various concentrations, from pure graphene to pure hBN, were also prepared. These stacked hybrid materials show interesting electrical, mechanical and optical properties distinctly different from pure graphene and hBN.[144]

One common characteristic of vertical heterostructures composed of small lattice mismatch materials is the appearance of moiré patterns (superlattices). As an example, moiré patterns in G/hBN heterostructures have been widely investigated. The layer by layer transfer method allows the formation of graphene and BN stacks with random rotation angles, which further leads to moiré patterns with different wavelengths (Fig. 8a). Fig. 8b shows the wavelength of the moiré pattern (black) and rotation angle (red) as a function of the lattice rotation angle φ between hBN and graphene. Due to the 1.8% lattice mismatch, a maximal moiré wavelength of about 14 nm is expected for graphene and hBN with a 0° lattice rotation.[5]

The moiré pattern, as a weak periodic potential, may result in the electronic structure of the heterostructures being different from their original components. For example, the moiré pattern of G/hBN stacks can introduce superlattice minibands or a small gap in graphene's band structure.[5,154] The inset of Fig. 8c displays one possible reconstructed band spectrum for graphene on hBN. These minibands can be observed by transport measurements when the lattice mismatch angle is less than 1°. Experimentally, the lattice alignment can be realized by the mechanical transfer method with the identification and alignment of the crystallographic edges of the graphene and hBN crystallites.[6,7] The inset of Fig. 8d shows the moiré pattern of the aligned graphene and hBN. Fig. 8c shows the typical behavior of the longitudinal resistivity *versus* the carrier density n. In addition to the usual resistance peak at the main charge neutrality point, two additional resistance peaks appear symmetrically. These extra neutrality points are attributed to the minibands resulting from superlattice potential induced by the hBN. Furthermore, in Fig. 8d, we can see the Hall resistance changes sign and passes through zero

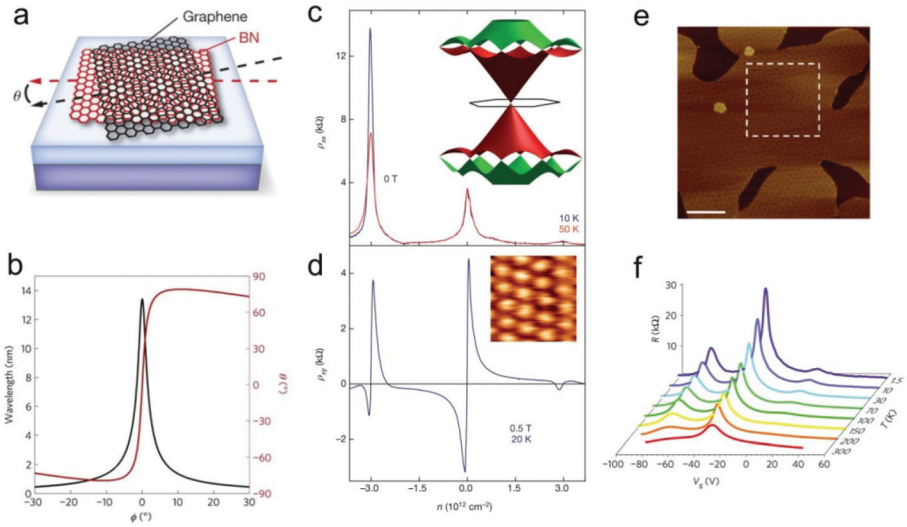

Fig. 8 Moiré superlattice and transport properties in G/hBN heterostacks. (a) Schematic of the Moiré pattern formation. The Moiré wavelength varies with the mismatch angle.[6] (b) Superlattice wavelength (black) and rotation (red) as a function of the angle between the graphene and hBN lattices.[5] (c, d) Transport properties of Dirac fermions in moiré superlattices. (c) Longitudinal resistivity as a function of *n*. Positive and negative values of *n* correspond to electrons and holes, respectively. Inset shows one possible spectrum of graphene on hBN. (d) Hall resistivity as a function of *n*. The Hall resistivity changes sign at high electron and hole doping. Inset is an AFM image showing the moiré pattern.[7] (e, f) Moiré superlattice in epitaxially grown G/hBN stacks. (e) AFM image of the grown G/hBN stacks, showing a trigonal moiré pattern. (f) Resistance *versus* V_g at various *T* of the G/hBN superlattice.[141] Reprinted with permission from: (a), ref. 6, © 2013 NPG; (b), ref. 5, © 2012 NPG; (c, d), ref. 7, © 2013 NPG; (e, f), ref. 141, © 2013 NPG.

near the neutrality points where the additional longitudinal resistance peaks appear.[7]

Moiré superlattice effects can also be observed in 2D stacks fabricated by direct growth method. Yang *et al*. observed a trigonal moiré pattern in graphene grown on hBN flakes by AFM (Fig. 8e). It was noted that all the moiré patterns of different graphene grains followed the same orientation, indicating that different graphene grains form a single crystal. The measured moiré periodicity is 15 ± 1 nm, which is in agreement with the modelling result of 14 nm with a zero rotation angle. The typical resistance behavior of monolayer graphene (Fig. 8f) also shows two additional peaks at both sides of the main peak, which are attributed to new Dirac points induced by the moiré superlattice potential; such an interpretation is in agreement with the calculated energy dispersion spectrum of graphene epitaxially grown on hBN with a zero rotation angle.[141]

In addition to the long-range superlattice potential effect, the interaction of the graphene and the closely aligned hBN also allows the band gap opening in graphene due to the local breaking of the carbon sublattice symmetry,[11,155–157] and thus, a higher "ON/OFF" ratio can be expected in these vertical devices, compared to pristine graphene electronic devices. Furthermore, unlike the doped-hBNC materials system, graphene's extremely high carrier mobility in these vertical heterostructures can be sustained due to the preservation of the structural integrity. Theoretically, G/hBN stacks, hBN/G/hBN sandwich structures, and G-hBN superlattices with a particular stacking order have been considered, and the finite band gaps have been predicted in these structures.[155–164] However, experimental realization of these graphene and hBN heterostructures remains a great challenge. Again, the direct CVD growth method may shed light on realizing the lattice alignment in these 2D heterostructures.

3.2.2. TMD-TMD stacks. Nearly lattice-matched TMDs based vertical heterostructures constitutes another material system that is currently receiving considerable attention, both in the theoretical and in experimental aspects. Theoretically, a large variety of TMD heterobilayers with different stacking orders were calculated. It was found that the electronic structures and optical properties of the new artificial stacks are modified to be different from that of pristine TMD layers.[165–170] For example, Terrones *et al*. demonstrated that a direct band gap ranging from 0.79 eV to 1.16 eV can be realized in TMD heterobilayers with particular stackings. It is important to note that in this direct band gap, electrons and holes are physically separated and localized in different layers.[165] Furthermore, it has been demonstrated that the moiré pattern in the $MoS_2/MoSe_2$ heterobilayer caused by a lattice mismatch or rotation can also have a significant effect on the electronic structures of the 2D heterostructures.[167] Therefore, band gap engineering could be realized in these TMD heterostructures, which could further provide opportunities for the construction of novel electronic and optoelectronic devices.

Experimentally, TMD-based vertical heterostructures were synthesized many years ago, using the van der Waals epitaxy (VDWE) method. VDWE refers to the growth of layered materials onto clean surfaces with no dangling bond, even if there is a large lattice mismatch between the two layers. The

resulting heterostructures are held together by weak van der Waals forces. Moreover, due to the absence of a dangling bond, the surface defects will be significantly reduced, resulting in a high-quality interface. The first layered materials produced by VDWE can be dated back to 1985 when Koma *et al.* grew ultrathin $NbSe_2$ and $MoSe_2$ on the cleaved face of MoS_2 single crystals by VDWE.[171] Very sharp and defect-free interfaces were found in their sample. Since then, many TMD layers and their heterostructures have been produced by the VDWE method, and which have been summarized in a recent review.[13]

The successful isolation of pristine TMD atomic layers from their bulks, allows the fabrication of ultrathin TMD-based vertical heterostructures *via* a sequential transfer method as mentioned earlier, similar to the graphene and hBN system. Fig. 9a shows an optical image of a WSe_2/MoS_2 heterobilayer. The rotated diffraction patterns shown in Fig. 9b along the [001] zone axis indicate a 12.5° rotation between the two lattices, therefore, the moiré pattern can be clearly observed in the HRTEM image, as shown in Fig. 9c. Photoluminescence (PL) and absorption spectroscopy were used to investigate the optoelectronic properties of the WSe_2/MoS_2 heterobilayer. As shown in Fig. 9d, a striking shift ~100 meV between the PL and absorbance peaks was observed. Due to the band offset of MoS_2 and WSe_2 (Fig. 9e), the optically excited excitons relax at the MoS_2/WSe_2 interface before recombination, thus resulting in a lower PL excitonic peak energy.[172] More recently, WS_2/MoS_2 heterostructures were prepared by transferring CVD-grown monolayer WS_2 onto MoS_2. It was shown that in such vertical heterostructures, the interlayer interaction could be tuned from noncoupling to strong coupling by thermal annealing.[173]

In addition to the transfer method, TMD stacks can also be fabricated *via* a vapor-phase growth method. A recently demonstrated example of this is the synthesis of WS_2/MoS_2 heterobilayers, which was achieved by the sequential sulfurization of transition metal oxides. MoO_3, WO_3, and S as the precursors were loaded into the furnace at the same time. Due to the large difference in melting points of MoO_3 and WO_3, it is possible to realize a sequential growth by controlling the temperature; that is, the MoS_2 monolayer is grown first on the substrates and then the WS_2 monolayer is grown on top of it. The fast Fourier transformation (FFT) from the STEM images in the WS_2/MoS_2 junction area showed identical hexagonal diffraction spots, which confirmed that the two monolayers have the same crystallographic orientation.[174]

In short, TMD stacks will bring more opportunities, not only because of the flexible choice of TMD layers, but also because of the unique structures and physical properties of these 2D layers. For example, their similar crystal structures and growth conditions ensure the possibility of synthesizing large-size hybrid structures using the CVD method. The band gap variations in the TMD layers (0.1–3 eV, from half-metal to semiconductors) provide different elements for multiple purposes. These new architectures may contribute greatly to future electronic and optoelectronic devices.

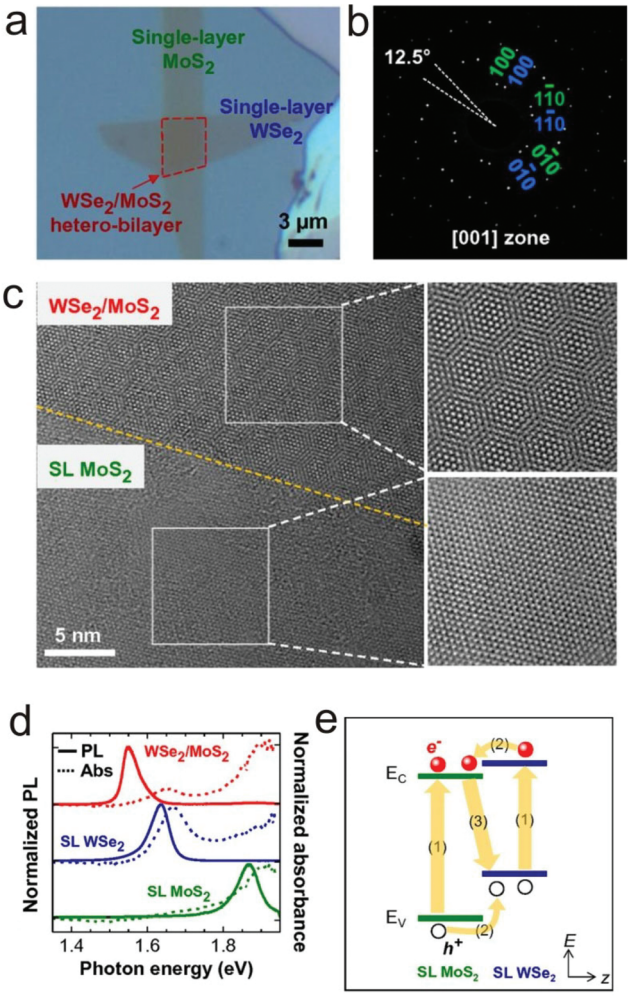

Fig. 9 Characterization of WSe_2/MoS_2 stacks. (a) Optical microscope image of a WSe_2/MoS_2 heterostructure on a SiO_2/Si substrate. (b) The electron diffraction pattern of the heterobilayer shown in a, with the pattern of MoS_2 and WSe_2 indexed in green and blue colors, respectively. (c) HRTEM images of a boundary region of monolayer MoS_2 and the heterobilayer, showing the moiré pattern. (d) Normalized PL (solid lines) and absorbance (dashed lines) spectra of monolayer WSe_2, MoS_2, and WSe_2/MoS_2 stacks. (e) Band diagram of WSe_2/MoS_2 heterobilayer under photoexcitation.[172] Reprinted with permission from ref. 172, © 2014 National Academy of Sciences.

3.2.3. Graphene and TMD (G-TMD) stacks. Graphene and TMDs have distinct properties but can be integrated into hybrid structures to realize novel functionalities. Recently, it has been demonstrated that vertical G/TMD/G stacks show great promise in high "ON/OFF" ratio FET, and in high performance optoelectronic and photovoltaic devices.[8–10,175] Here, we review recent experiments on the fabrication of G-TMD vertical heterostructures.

G-TMD stacks can be prepared by transferring and stacking individual layers. The technique for growing large-area graphene and MoS_2 films allows the fabrication of large-area G-MoS_2 stacks by a PMMA-assisted transfer method, as shown in Fig. 10a.[139] In addition to direct transfer, other procedures have also been developed to synthesize G-MoS_2 vertical hetero-

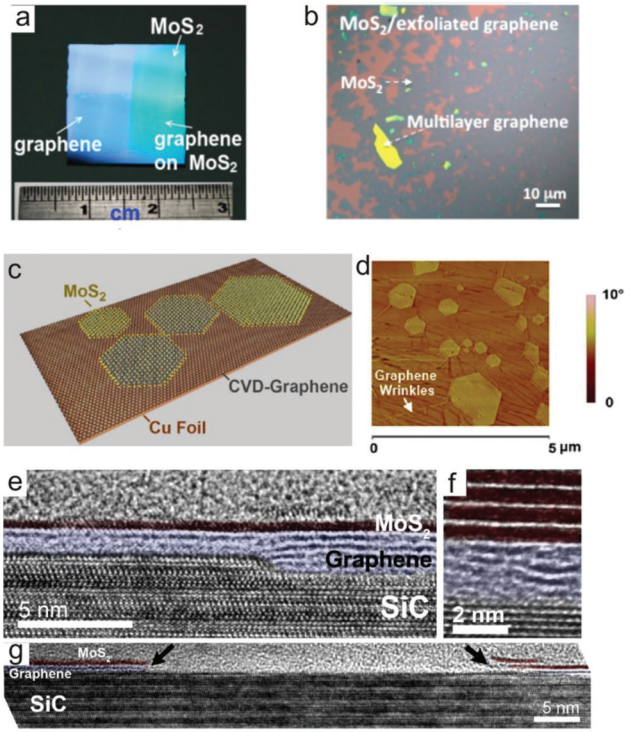

Fig. 10 Synthesis of MoS_2 and graphene stacks. (a) Photo of a large-area graphene on a MoS_2 stack fabricated by the transfer method.[139] (b) Optical image of MoS_2 layers grown on exfoliated graphene with $F_{16}CuPc$ as a seeding promoter.[109] (c) Schematic illustration and (d) AFM phase images of MoS_2 layers grown on graphene by VDWE.[177] (e–g) Cross-sectional HRTEM images of MoS_2 grown on: (e) flat graphene, (f) defective graphene, and (g) SiC partially covered by graphene.[137] Reprinted with permission from: (a), ref. 139, © 2014, rights managed by NPG; (b), ref. 109, © 2014 ACS; (c, d), ref. 177, © 2012 ACS; (e–g), ref. 137, © 2014 ACS.

structures. Ling *et al*. found that MoS_2 growth from sources of MoO_3 and S powders can be promoted by using aromatic molecules as seeds on various substrates. They demonstrated that MoS_2 layers tend to grow on bare SiO_2/Si substrates rather than on graphene or hBN substrates. However, when using $F_{16}CuPc$ as a seed, $F_{16}CuPc$ can stay on graphene or the hBN surface at a growth temperature of 650 °C. After growth, monolayer MoS_2 is found to be formed on graphene and hBN flakes (Fig. 10b).[109] Recently, Fu *et al*. prepared large-area G/MoS_2 (graphene on MoS_2) heterostructures by heating Mo–oleate complex coated sodium sulfate under a N_2 atmosphere.[176]

VDWE has been used for the preparation of high-quality G-TMD stacks. Shi *et al*. demonstrated the VDWE growth of few layer MoS_2 on a CVD-graphene/Cu foil substrate using $(NH_4)_2MoS_4$ as a precursor (Fig. 10c and d).[177] They believed that the surface of CVD-graphene is free of dangling bonds, which makes it possible for the growth of lattice-mismatched MoS_2 on it *via* weak van der Waals forces. They investigated the orientation relationship of CVD-grown MoS_2 and the underlying graphene substrate using SAED, and found that though the grown monolayer MoS_2 film is polycrystalline, a large fraction of the MoS_2 grains grew with the same orientation as the underlying graphene. However, it is still a great challenge to control the MoS_2 layer numbers in the stack when using $(NH_4)_2MoS_4$ as a precursor. In addition, epitaxial graphene grown on 6H-SiC (0001) free of dangling bonds was identified as an ideal substrate for various van der Waals heterostructures formation. The vapor-phase growth of MoS_2, WSe_2, and hBN using MoO_3, WO_3, S, Se, and ammonia borane powders was found to be compatible with graphene/SiC substrates, thus leading to the formation of hBN/G and TMD/G stacks. It was found that the structures of the underlying graphene determined the nucleation behavior of MoS_2. A flat graphene surface supports uniform MoS_2 growth on top (Fig. 10e), while wrinkles/defects on the surface of graphene promote the growth of MoS_2 adlayers (Fig. 10f). However, MoS_2 nucleation cannot be observed on the bare SiC (0001) surface without graphene (Fig. 10g). Furthermore, from the HRTEM image, we note that the grown MoS_2/G stacks exhibits atomically sharp interfaces, which indicates that the direct growth method may also lead to high-quality 2D heterostacks.[137] Recently, Shim *et al*. reported the growth of $MoSe_2$/G heterostructures, and they found that the photo-generated charge carriers in $MoSe_2$ can be readily transferred to graphene, leading to quenching of the PL intensity in monolayer $MoSe_2$.[98]

In addition to the vertical heterostructures discussed above, there are also a large number of other stacks that have been prepared. VDWE is an effective way to obtain diverse heterostructures. To date, graphene, graphite, hBN, mica, and many TMD crystals have been used as good substrates for VDWE, upon which other types of 2D materials, such as topological insulator layers, can be grown. Dang *et al*. reported the VDWE growth of ultrathin topological insulator Bi_2Se_3 nanoplates with defined orientations on exfoliated few-layer graphene by a catalyst-free vapor-phase transport method.[178] Similarly, Gehring *et al*. prepared Bi_2Te_2Se nanoplatelets on exfoliated hBN. The mobility of Bi_2Te_2Se on hBN was greatly enhanced compared to Bi_2Te_2Se on SiO_2/Si substrates.[179] In addition, other layered heterostructures, such as MoS_2/SnS_2,[180] TaS_2/hBN,[181] TaS_2/mica,[181] MoS_2/mica,[108] $MoSe_2(NbSe_2)$/mica,[182] $Bi_2Se_3(Bi_2Te_3)$/mica,[183] and Te/mica,[184] *etc*., were also reported experimentally. Furthermore, by using the well-developed sequential transfer method, one can stack arbitrary stable 2D materials together to form heterostructures. Recently, many other new 2D members (silicene,[185–188] phosphorene,[189,190] *etc*.) with novel properties have been successfully prepared, providing great opportunities for future 2D heterostructures research, *e.g.* for optoelectronic devices based on vertical p–n junctions by stacking p-type phosphorene and n-type TMDs.[191]

4. Application

Because of their unique properties, such as strong electron–hole confinement, extreme bendability, and high transparency, 2D materials have attracted significant interest for both fundamental research and in practical applications.[15,192] In addition

to the research on individual graphene-like 2D materials, a lot of effort has also been focused on the hybrid heterostructures and devices of 2D materials.[12,19] Creating artificial heterostructures *via* stacking different 2D crystals on top of each other establishes a whole family of new materials with unusual characteristics and exciting possibilities for novel 2D devices. In the following section, we will review the applications of 2D heterostructures in the field of electronic and optoelectronic devices.

4.1. Electronic devices

Since the first report of graphene and its electric field effect,[3] graphene has been one of the hottest research topics in electronic devices applications.[193] The absence of an energy gap limits the "ON/OFF" ratio in graphene transistors. Therefore, various approaches, such as using bilayer graphene,[194,195] nanoribbons,[196] or quantum dots,[197] have been adopted to open the band gap of graphene, but to date, they all result in the degradation of the electron transport properties of graphene. Alternatively, heterostructures based on graphene and other 2D materials provide opportunities to design novel device structures for electronic application.[8,19,136,198] Because of the atomic layer thickness of each layer in the vertically stacked 2D heterostructures, the heterointerface can be tuned by gate voltage. Britnell *et al*. reported a field effect tunneling transistor (FETT) based on vertical graphene heterostructures.[8] The atomically thin hBN or MoS_2 layer acts as a barrier layer between two graphene layers, as shown in Fig. 11a and b. By applying a gate voltage between the Si substrate and the bottom graphene layer, the Fermi level in the graphene layers could be tuned, resulting in the tenability of the tunneling current. Because of the wide band gap of hBN (5–6 eV), the barrier height formed in the G/hBN/G FETTs is much higher than the change of Fermi level in graphene, which leads to the low "ON/OFF" ratio of the FETT. Instead of hBN, Georgiou *et al*. used WS_2 as the barrier materials in FETTs.[10] WS_2 has a relatively small band gap (1.4 eV) and only a weak impurity band, which allows for switching between tunneling and thermionic transport regimes. The G/WS_2/G FETTs exhibit much better transistor characteristics, including an "ON/OFF" ratio of 10^6 and a high "ON" current. The mechanism of charge transport in vertical stacked heterostructures depends on the thickness of the barrier layer. When the barrier layer is thinner, the tunneling current is the dominant component in charge transport; here, the transistor shows a high current density but low "ON/OFF" current ratio. For thicker barrier layers or when applying lager gate voltage, the charge transport is dominated by the thermionic emission through the Schottky barrier.[199] In addition, the stacked heterostructure is only a few atomic layers thick, so bending has almost no effect on the transistor performance, which makes it suitable for transparent and flexible electronics.

The polarity of the vertically stacked transistor can also be obtained by incorporating different layered materials between the graphene layers. For example, by inserting $Bi_2Sr_2CO_2O_8$ between the graphene layers, the vertically stacked devices show p-channel characteristics. A complementary inverter based on graphene, $Bi_2Sr_2CO_2O_8$ (p-channel), graphene, MoS_2 (n-channel), and a metal thin film vertically stacked heterostructure has been demonstrated with a larger-than-unity voltage gain (Fig. 11c and d). The vertically stacked heterostructure opens up a new dimension for the high-density integration of functional devices and circuits.

Except for FETT devices, heterostructures have also been used in other applications, such as in memory cells. By combining the unique electric properties of monolayer MoS_2 with the conductivity of graphene, 2D heterostructures capable of information storage have been demonstrated by Bertolazzi *et al*.[201] The memory device utilizes MoS_2 and graphene as the channel and ohmic electrodes, respectively, with a charge trapping layer in the form of a few-layer graphene floating gate. A factor of 10^4 difference between the memory program and erase states was achieved, because of the high sensitivity of the monolayer MoS_2 to the presence of charges in the charge trapping layer. Choi *et al*. also studied similar memory cells, using hBN, instead of HfO_2, as the barrier layer, as shown in Fig. 11e and f.[200] In their case, two types of the memory devices were compared: one with graphene as the FET channel, hBN as the tunnel barrier, and MoS_2 as the charge trapping layer; and the other with MoS_2 as the FET channel, hBN as the tunnel barrier, and graphene as the charge trapping layer. By varying the thicknesses of 2D materials and by modifying the stacking order, the hysteresis and conductance polarity of the memory cell could be controlled. Although a 2D materials-based stacked heterostructure can provide a platform for future flexible and transparent memory device operations, numerous scientific challenges, such as the development of integrated memory cell arrays with ultra-large density and low power consumption, need to be considered in the future.

Compared with the vertical stacked heterostructures discussed above, fabrication of a lateral structure is still a big challenge. Recent advances in the CVD growth of both graphene and hBN have enabled the precise fabrication of G-hBN lateral structures. A G-hBN lateral structure with atomic lattice coherence can be formed by either the direct growth of hBN at the edge of graphene, or by chemically converting graphene to hBN. Electronic devices based on G-hBN lateral structures have also been investigated, such as field effect transistors, resonators, *etc*. By changing the concentration of carbon in the channel, the mobility and the "ON/OFF" ratio of the device can be tuned. Because of the insulating properties of hBN, electrically isolated graphene devices can be fabricated in a single, atomically flat sheet based on the G-hBN lateral structure, as shown in Fig. 11g and h.[117] Such hybrid structures are particularly useful for ultraflat three-dimensional electronics.

4.2. Optoelectronic devices

Due to the direct band gap, strong photoluminescence, and large exciton binding energy, monolayer TMDs are promising materials for optoelectronic application,[202,203] such as photodetectors,[203,204] light-emitting devices,[205,206] and photo-

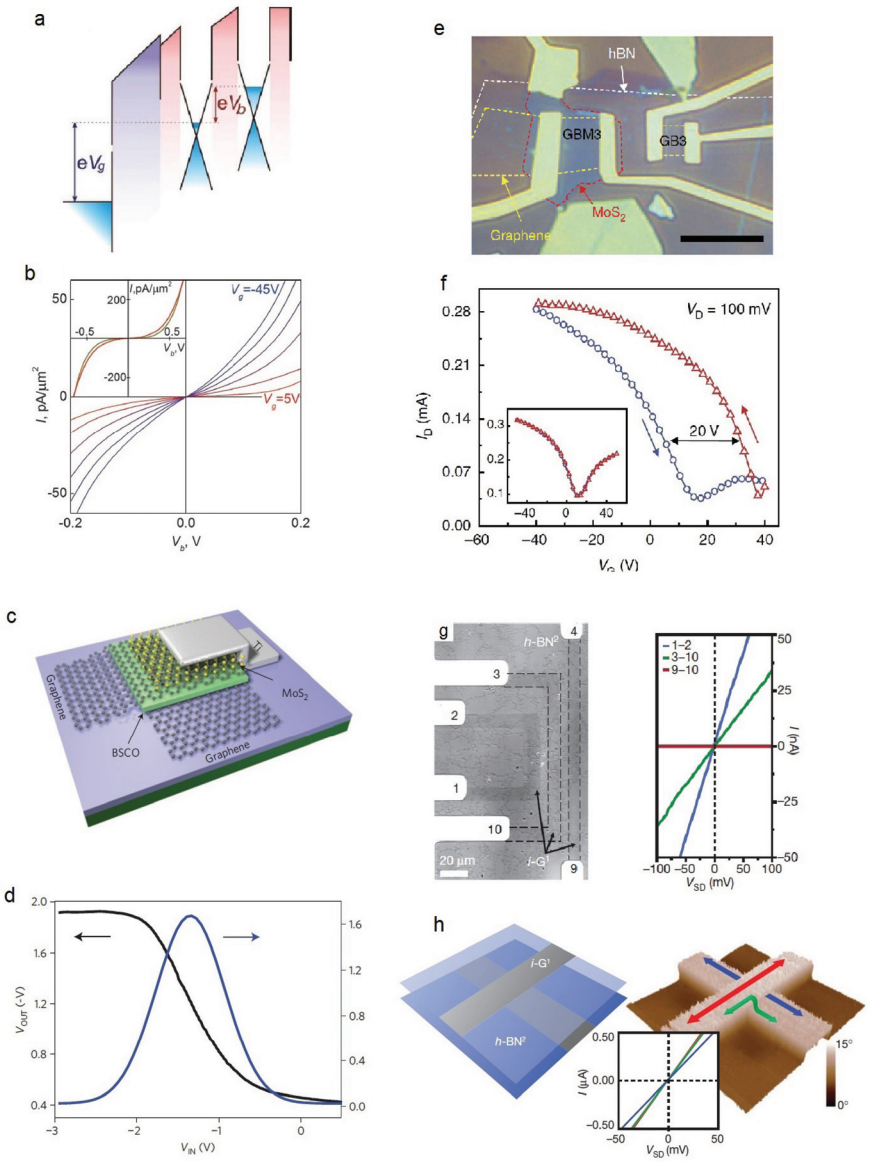

Fig. 11 Electronic device of graphene-based 2D heterostructures. (a) Band structure of G/hBN/G heterostructure under finite gate (V_g) and bias voltage (V_b). (b) I–V characteristics for a typical G/hBN/G FETT.[8] (c) Three-dimensional schematic illustration of a complementary inverter by vertically stacking graphene, p-type $Bi_2Sr_2Co_2O_8$, graphene, n-type MoS_2, and a metal thin film. (d) The inverter characteristics from the device shown in (c), with an inverter gain of about 1.7.[199] (e) Optical images of a heterostructured memory device based on G/hBN/MoS_2. (f) Transfer characteristic of the memory device shown in (e).[200] (g) The left panel is the optical image of a G-hBN lateral heterostructure with electrodes contacting graphene strips. The right panel is the I–V characteristics of the indicated devices in the left panel. (h) Schematic and electrostatic force microscopy (EFM) image of a graphene–graphene cross-junction fabricated by transfer process. The inset shows the I–V characteristics.[117] Reprinted with permission from: (a, b), ref. 8, © 2012 AAAS; (c, d), ref. 199, © 2013 NPG; (e, f), ref. 200, © 2013 NPG; (g, h), ref. 117, © 2012 NPG.

voltaics.[207] Engineering the electronic properties of TMDs by designing heterostructures provide a much wider range of candidates for optoelectronic applications. In this section, we focus on the application of heterostructures in photodetectors, photovoltaics and light-emitting devices.

Combining fast response time, due to the high mobility of graphene, and strong light absorption, due to large direct band gap of MoS_2, photodetectors based on vertical G/MoS_2 stacks have shown a very high photogain, greater than 10^8.[139] Due to the presence of a perpendicular effective electric field, the photoelectrons produced in the MoS_2 layer after light absorption are subsequently injected into the graphene layer, rather than trapped in MoS_2. A similar mechanism has also been applied to other semiconductors, such as graphene-quantum dot hybrid heterostructures.[208] Besides the high photoresponsivity, a gate-tunable persistent photoconductivity was also observed in the G/MoS_2 heterostructure, as shown in Fig. 12a and b.[209] The persistent photocurrent is due to a combined effect of carrier localization in MoS_2 and the external gate electric field.

With analogy to the FETT device, the light-matter interaction in vertically stacked heterostructures was also studied. 2D heterostructures consisting of TMDs sandwiched between graphene sheets exhibit a photoresponsivity of 0.1 A W^{-1}, which is because the Van Hove singularities in the electronic density of states of TMDs guarantees enhanced light-matter interactions, leading to enhanced photon absorption and an electron–hole creation.[9] Recently Yu *et al*. demonstrated a way to control the photocarrier generation, and the separation and transport processes using an external electric field in the G/MoS_2/G vertical heterostructure.[175] They showed that the amplitude and polarity of the photocurrent in the gated vertical heterostructures can be readily modulated by the electric field of an external gate to achieve a maximum external quantum efficiency of 55%. More recently, high photoresponsivity has been achieved in all-graphene bilayer vertical heterostructures.[210,211] Two graphene layers are separated by a thin barrier layer, and a photocurrent is generated from the tunneling current through the interlayer formed between the p- and n-type doped graphene layers, or from the strong photogating effect.

p–n junctions are the essential elements for optoelectronic devices. Although the vertical heterostructures have been extensively studied, p–n junctions based on the same 2D semiconductor are relatively unexplored, due to the difficulty in the p-type doping of 2D materials. The p–n junctions consisting of n-type 2D materials and p-type conventional semiconductors have been investigated. Electroluminescence has been observed in monolayer MoS_2 and p-type silicon p–n junctions, as shown in Fig. 13a and b.[212] A carbon nanotube–MoS_2 heterojunction p–n diode responds strongly to optical irradiation, with an external quantum efficiency of 25% and a fast photoresponse of about 15 μs.[213]

Furthermore, scientists have tried to individually contact layers of p-type WSe_2 and n-type monolayers or few-layer TMDs (MoS_2, WS_2) to create an atomically thin p–n junction with the type II band alignment.[172,214–216] Here, excellent diode characteristics with well-defined current rectification behavior were demonstrated in these devices, as shown in Fig. 13c and d.[172] Besides the rectifying current–voltage characteristics, the p–n junction can also be used in other optoelectronic devices. A photovoltaic response has been observed across the p–n interface, and the collection of photocarriers can be enhanced by sandwiching the atomic p–n junction between graphene layers.[215] An electrically driven light emitter has also been demonstrated, in which electroluminescence originated from the exciton emission and hot electron luminescence.[214]

The p–n junctions discussed above are mainly vertically stacked heterostructures. Lateral p–n junctions have been a big challenge, due to the precise control over the growth and due to the lattice matching issues. Because of the ambipolar behavior of some TMDs, p–n junctions can be formed in the lateral plane by electrostatic doping. The first lateral p–n junction was formed by the ionic gating of MoS_2 under specific conditions.[218] p–n junctions based on a WSe_2 monolayer have been demonstrated independently by several groups.[217,219,220] As shown in Fig. 13e and f, in these structures two separated gates are used to form the p- and n-type doping regime, which

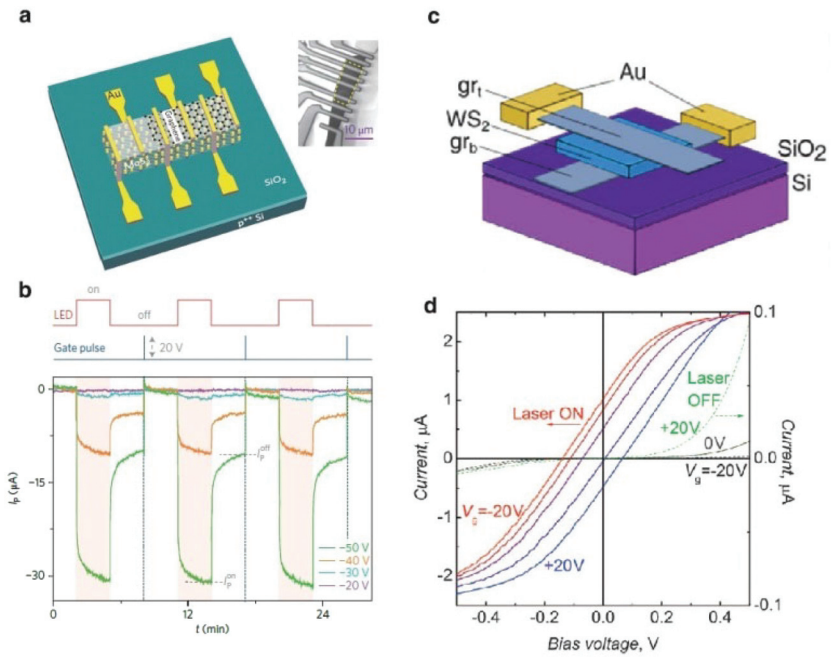

Fig. 12 Photoresponse properties of 2D heterostructure-based devices. (a) Schematic of the vertical G/MoS_2 device architecture, (b) Photocurrent induction and switching operation of the G/MoS_2 device under different gate voltages. The vertical shaded columns and blue (dotted) lines indicate the presence of light and the application of gate pulses, respectively.[209] (c) Schematic of the G/WS_2/G device. (d) *I*–*V* curves for a device taken under illumination (left axis) and in the dark (right axis) at different gate voltages after doping.[9] Reprinted with permission from: (a, b), ref. 209, © 2013 NPG; (c, d), ref. 9, © 2013 AAAS.

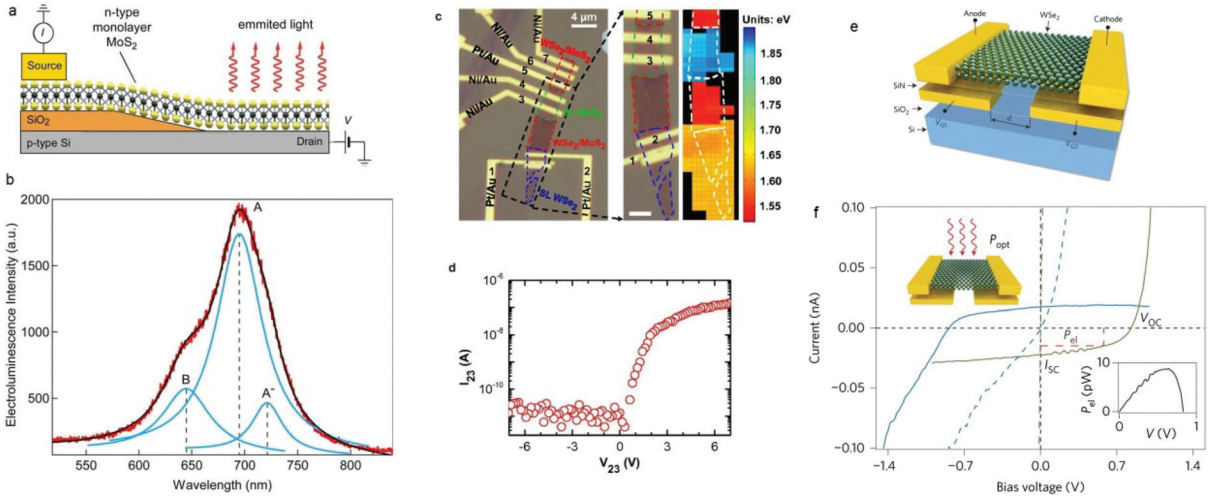

Fig. 13 Optoelectronic devices based on 2D p–n junctions. (a) Cross-sectional view of the structure of the MoS_2/Si heterostructure device. (b) Electroluminescence spectrum and fitting of the MoS_2/Si heterostructure.[212] (c) Optical image of the monolayer WSe_2, WSe_2/MoS_2 heterostructures, and monolayer MoS_2. (d) *I*–*V* characteristic of the WSe_2/MoS_2 heterostructure.[172] (e) Schematic of a monolayer WSe_2 device with split gate electrodes. (f) *I*–*V* characteristics of the device under optical illumination for different biasing conditions.[217] Reprinted with permission from: (a, b), ref. 212, © 2014 ACS; (c, d), ref. 172, © 2014 National Academy of Sciences; (e, f), ref. 217, © 2014 NPG.

allows them to operate as light emitting diodes, photovoltaic solar cells, and photodetectors under different bias condition.

Although extensive research has been focused on 2D heterostructures in recent years, device applications remain largely unexplored. The flat and dangling-bond-free surfaces of 2D crystals allows the on-demand fabrication of heterojunctions with the desired band alignment, using a library of numerous 2D metallic, semiconducting, or insulating 2D layers, revealing unusual properties and new phenomena. Further optimization of the band alignment, fabrication techniques, and interface lattice mismatching will lead to the design of new devices with novel functionalities, such as valley-based electronics and optoelectronic devices.[221,222]

5. Conclusion and outlook

Great achievements in graphene and graphene analogues have stimulated the exploration of 2D heterostructures ever since the discovery of graphene. These studies have brought us to a brave new world of 2D materials and their heterostructures. In this review, we have summarized recent progress on the fabrication, characterization, and applications of 2D vertical and lateral heterostructures.

Vapor-phase growth has been recognized as a most effective way to obtain high quality graphene, hBN, TMDs, *etc*. Recently, increasing research has shown that direct growth could also serve as an important method of 2D heterostructures fabrication. More importantly, this routine could lead to the formation of heterostructures consisting of lattice aligned 2D layers with atomically sharp interfaces, for both vertical and lateral cases, as confirmed by the graphene and hBN system. In the last section, we reviewed recent progress on the applications of atomically thin 2D heterostructures. It has been demonstrated that 2D heterostructures can find promising applications in high-mobility electronics, tunneling FET, memory devices, photodetectors, *etc*.

Although in the past few years significant effort has been poured into this emerging field of 2D heterostructures, there still exist a number of significant issues that need to be addressed and explored. The first challenge will be the large-area fabrication. Surely, at present, 2D heterostructures prepared by exfoliation-transfer technique seem good only for lab studies, and a more scalable fabrication approach is highly desirable. To this end, direct growth as a promising way needs to be further explored to produce large-area and high-quality heterostructures in a controlled manner. In addition, with the improvement of fabrication and transfer techniques, other unique heterostructures may be designed by finely tuning the parameters, like band alignment, lattice mismatch, *etc*. For example, by utilizing strong spin–orbital coupling in TMDs, novel valleytronics-based heterostructure devices are highly expected. Considering that increasing numbers of 2D layers with distinct properties have been synthesized and isolated experimentally, it will be quite exciting to expect what will be brought to us in the future by the kaleidoscopic landscapes of those amazing 2D layers and their heterostructures.

Competing financial interests

The authors declare no competing financial interests.

Acknowledgements

This work is supported by the Singapore National Research Foundation under NRF RF Award no. NRF-RF2013-08, the

start-up funding from Nanyang Technological University (M4081137.070). This work is supported by National Natural Science Foundation of China (grant no. 61422501 and 11374023), the National Basic Research Program of China (973 Program), grant no. 2015CB932400, and Beijing Natural Science Foundation (grant no. L140007). This research is supported in part by a Wigner Fellowship through the Laboratory Directed Research and Development Program of Oak Ridge National Laboratory (ORNL), managed by UT-Battelle, LLC, for the U. S. DOE (WZ), and through a user project supported by ORNL's Center for Nanophase Materials Sciences (CNMS), which is sponsored by the Scientific User Facilities Division, Office of Basic Energy Sciences, U. S. DOE.

References

1 R. E. Peierls, *Ann. I. H. Poincare*, 1935, **5**, 177–222.
2 L. D. Landau, *Phys. Z. Sowjetunion*, 1937, **11**, 26–35.
3 K. S. Novoselov, A. K. Geim, S. V. Morozov, D. Jiang, Y. Zhang, S. V. Dubonos, I. V. Grigorieva and A. A. Firsov, *Science*, 2004, **306**, 666–669.
4 C. R. Dean, A. F. Young, I. Meric, C. Lee, L. Wang, S. Sorgenfrei, K. Watanabe, T. Taniguchi, P. Kim, K. L. Shepard and J. Hone, *Nat. Nanotechnol.*, 2010, **5**, 722–726.
5 M. Yankowitz, J. Xue, D. Cormode, J. D. Sanchez-Yamagishi, K. Watanabe, T. Taniguchi, P. Jarillo-Herrero, P. Jacquod and B. J. LeRoy, *Nat. Phys.*, 2012, **8**, 382–386.
6 C. R. Dean, L. Wang, P. Maher, C. Forsythe, F. Ghahari, Y. Gao, J. Katoch, M. Ishigami, P. Moon, M. Koshino, T. Taniguchi, K. Watanabe, K. L. Shepard, J. Hone and P. Kim, *Nature*, 2013, **497**, 598–602.
7 L. A. Ponomarenko, R. V. Gorbachev, G. L. Yu, D. C. Elias, R. Jalil, A. A. Patel, A. Mishchenko, A. S. Mayorov, C. R. Woods, J. R. Wallbank, M. Mucha-Kruczynski, B. A. Piot, M. Potemski, I. V. Grigorieva, K. S. Novoselov, F. Guinea, V. I. Fal'ko and A. K. Geim, *Nature*, 2013, **497**, 594–597.
8 L. Britnell, R. V. Gorbachev, R. Jalil, B. D. Belle, F. Schedin, A. Mishchenko, T. Georgiou, M. I. Katsnelson, L. Eaves, S. V. Morozov, N. M. R. Peres, J. Leist, A. K. Geim, K. S. Novoselov and L. A. Ponomarenko, *Science*, 2012, **335**, 947–950.
9 L. Britnell, R. M. Ribeiro, A. Eckmann, R. Jalil, B. D. Belle, A. Mishchenko, Y.-J. Kim, R. V. Gorbachev, T. Georgiou, S. V. Morozov, A. N. Grigorenko, A. K. Geim, C. Casiraghi, A. H. C. Neto and K. S. Novoselov, *Science*, 2013, **340**, 1311–1314.
10 T. Georgiou, R. Jalil, B. D. Belle, L. Britnell, R. V. Gorbachev, S. V. Morozov, Y.-J. Kim, A. Gholinia, S. J. Haigh, O. Makarovsky, L. Eaves, L. A. Ponomarenko, A. K. Geim, K. S. Novoselov and A. Mishchenko, *Nat. Nanotechnol.*, 2013, **8**, 100–103.
11 B. Hunt, J. D. Sanchez-Yamagishi, A. F. Young, M. Yankowitz, B. J. LeRoy, K. Watanabe, T. Taniguchi, P. Moon, M. Koshino, P. Jarillo-Herrero and R. C. Ashoori, *Science*, 2013, **340**, 1427–1430.
12 A. K. Geim and I. V. Grigorieva, *Nature*, 2013, **499**, 419–425.
13 S. Z. Butler, S. M. Hollen, L. Cao, Y. Cui, J. A. Gupta, H. R. Gutiérrez, T. F. Heinz, S. S. Hong, J. Huang, A. F. Ismach, E. Johnston-Halperin, M. Kuno, V. V. Plashnitsa, R. D. Robinson, R. S. Ruoff, S. Salahuddin, J. Shan, L. Shi, M. G. Spencer, M. Terrones, W. Windl and J. E. Goldberger, *ACS Nano*, 2013, **7**, 2898–2926.
14 C. Rao, H. Ramakrishna Matte and U. Maitra, *Angew. Chem., Int. Ed.*, 2013, **52**, 13162–13185.
15 M. Xu, T. Liang, M. Shi and H. Chen, *Chem. Rev.*, 2013, **113**, 3766–3798.
16 Y. Lin and J. W. Connell, *Nanoscale*, 2012, **4**, 6908–6939.
17 Q. H. Wang, K. Kalantar-Zadeh, A. Kis, J. N. Coleman and M. S. Strano, *Nat. Nanotechnol.*, 2012, **7**, 699–712.
18 K. J. Koski and Y. Cui, *ACS Nano*, 2013, **7**, 3739–3743.
19 C. Dean, A. F. Young, L. Wang, I. Meric, G. H. Lee, K. Watanabe, T. Taniguchi, K. Shepard, P. Kim and J. Hone, *Solid State Commun.*, 2012, **152**, 1275–1282.
20 C. Berger, Z. Song, T. Li, X. Li, A. Y. Ogbazghi, R. Feng, Z. Dai, A. N. Marchenkov, E. H. Conrad, P. N. First and W. A. de Heer, *J. Phys. Chem. B*, 2004, **108**, 19912–19916.
21 C. Li, D. D. Li, J. J. Yang, X. P. Zeng and W. X. Yuan, *J. Nanomater.*, 2011, 319624.
22 K. Nakatsuji, Y. Shibata, R. Niikura, F. Komori, K. Morita and S. Tanaka, *Phys. Rev. B: Condens. Matter*, 2010, **82**, 045428.
23 J. Hass, W. A. de Heer and E. H. Conrad, *J. Phys.: Condens. Matter*, 2008, **20**, 323202.
24 K. V. Emtsev, F. Speck, T. Seyller, L. Ley and J. D. Riley, *Phys. Rev. B: Condens. Matter*, 2008, **77**, 155303.
25 W. A. de Heer, C. Berger, X. S. Wu, P. N. First, E. H. Conrad, X. B. Li, T. B. Li, M. Sprinkle, J. Hass, M. L. Sadowski, M. Potemski and G. Martinez, *Solid State Commun.*, 2007, **143**, 92–100.
26 J. Kedzierski, H. Pei-Lan, P. Healey, P. W. Wyatt, C. L. Keast, M. Sprinkle, C. Berger and W. A. de Heer, *IEEE Trans. Electron Devices*, 2008, **55**, 2078–2085.
27 J. S. Moon, D. Curtis, M. Hu, D. Wong, C. McGuire, P. M. Campbell, G. Jernigan, J. L. Tedesco, B. VanMil, R. Myers-Ward, C. Eddy and D. K. Gaskill, *IEEE Electron Device Lett.*, 2009, **30**, 650–652.
28 A. Reina, X. T. Jia, J. Ho, D. Nezich, H. B. Son, V. Bulovic, M. S. Dresselhaus and J. Kong, *Nano Lett.*, 2009, **9**, 30–35.
29 M. S. Xu, D. Fujita, K. Sagisaka, E. Watanabe and N. Hanagata, *ACS Nano*, 2011, **5**, 1522–1528.
30 S. J. Chae, F. Gunes, K. K. Kim, E. S. Kim, G. H. Han, S. M. Kim, H. J. Shin, S. M. Yoon, J. Y. Choi, M. H. Park, C. W. Yang, D. Pribat and Y. H. Lee, *Adv. Mater.*, 2009, **21**, 2328–2333.
31 Y. S. Dedkov, M. Fonin, U. Rudiger and C. Laubschat, *Appl. Phys. Lett.*, 2008, **93**, 022509.

32 S. Garaj, W. Hubbard and J. A. Golovchenko, *Appl. Phys. Lett.*, 2010, **97**, 183103.
33 H. J. Park, J. Meyer, S. Roth and V. Skakalova, *Carbon*, 2010, **48**, 1088–1094.
34 S. Amini, J. Garay, G. X. Liu, A. A. Balandin and R. Abbaschian, *J. Appl. Phys.*, 2010, **108**, 094321.
35 T. Iwasaki, H. J. Park, M. Konuma, D. S. Lee, J. H. Smet and U. Starke, *Nano Lett.*, 2011, **11**, 79–84.
36 F. Gunes, G. H. Han, K. K. Kim, E. S. Kim, S. J. Chae, M. H. Park, H. K. Jeong, S. C. Lim and Y. H. Lee, *Nano*, 2009, **4**, 83–90.
37 N. Liu, L. Fu, B. Y. Dai, K. Yan, X. Liu, R. Q. Zhao, Y. F. Zhang and Z. F. Liu, *Nano Lett.*, 2011, **11**, 297–303.
38 R. Wang, Y. F. Hao, Z. Q. Wang, H. Gong and J. T. L. Thong, *Nano Lett.*, 2010, **10**, 4844–4850.
39 K. M. Reddy, A. D. Gledhill, C. H. Chen, J. M. Drexler and N. P. Padture, *Appl. Phys. Lett.*, 2011, **98**, 113117.
40 A. Srivastava, C. Galande, L. Ci, L. Song, C. Rai, D. Jariwala, K. F. Kelly and P. M. Ajayan, *Chem. Mater.*, 2010, **22**, 3457–3461.
41 L. Gao, J. R. Guest and N. P. Guisinger, *Nano Lett.*, 2010, **10**, 3512–3516.
42 H. I. Rasool, E. B. Song, M. J. Allen, J. K. Wassei, R. B. Kaner, K. L. Wang, B. H. Weiller and J. K. Gimzewski, *Nano Lett.*, 2011, **11**, 251–256.
43 A. W. Robertson and J. H. Warner, *Nano Lett.*, 2011, **11**, 1182–1189.
44 X. Li, W. Cai, J. An, S. Kim, J. Nah, D. Yang, R. Piner, A. Velamakanni, I. Jung, E. Tutuc, S. K. Banerjee, L. Colombo and R. S. Ruoff, *Science*, 2009, **324**, 1312–1314.
45 L. Gao, W. Ren, H. Xu, L. Jin, Z. Wang, T. Ma, L.-P. Ma, Z. Zhang, Q. Fu, L.-M. Peng, X. Bao and H.-M. Cheng, *Nat. Commun.*, 2012, **3**, 699.
46 B. J. Kang, J. H. Mun, C. Y. Hwang and B. J. Cho, *J. Appl. Phys.*, 2009, **106**, 104309.
47 T. Gao, S. Xie, Y. Gao, M. Liu, Y. Chen, Y. Zhang and Z. Liu, *ACS Nano*, 2011, **5**, 9194–9201.
48 G. Imamura and K. Saiki, *J. Phys. Chem. C*, 2011, **115**, 10000–10005.
49 H. Ago, Y. Ito, N. Mizuta, K. Yoshida, B. Hu, C. M. Orofeo, M. Tsuji, K. Ikeda and S. Mizuno, *ACS Nano*, 2010, **4**, 7407–7414.
50 G. E. Ramirez-Caballero, J. C. Burgos and P. B. Balbuena, *J. Phys. Chem. C*, 2009, **113**, 15658–15666.
51 E. Sutter, P. Albrecht and P. Sutter, *Appl. Phys. Lett.*, 2009, **95**, 133109.
52 P. W. Sutter, J. I. Flege and E. A. Sutter, *Nat. Mater.*, 2008, **7**, 406–411.
53 J. Coraux, A. T. N'Diaye, M. Engler, C. Busse, D. Wall, N. Buckanie, F. Heringdorf, R. van Gastel, B. Poelsema and T. Michely, *New J. Phys.*, 2009, **11**, 023006.
54 A. T. N'Diaye, J. Coraux, T. N. Plasa, C. Busse and T. Michely, *New J. Phys.*, 2008, **10**, 043033.
55 Y. Murata, E. Starodub, B. B. Kappes, C. V. Ciobanu, N. C. Bartelt, K. F. McCarty and S. Kodambaka, *Appl. Phys. Lett.*, 2010, **97**, 143114.
56 C. A. Di, D. C. Wei, G. Yu, Y. Q. Liu, Y. L. Guo and D. B. Zhu, *Adv. Mater.*, 2008, **20**, 3289–3293.
57 T. Oznuluer, E. Pince, E. O. Polat, O. Balci, O. Salihoglu and C. Kocabas, *Appl. Phys. Lett.*, 2011, **98**, 183101.
58 J. Fujita, R. Ueki, Y. Miyazawa and T. Ichihashi, *J. Vac. Sci. Technol., B*, 2009, **27**, 3063–3066.
59 F. Jun-ichi, M. Yosuke, U. Ryuichi, S. Mio and S. Takeshi, *Jpn. J. Appl. Phys.*, 2010, **49**, 06GC01.
60 G. Ding, Y. Zhu, S. Wang, Q. Gong, L. Sun, T. Wu, X. Xie and M. Jiang, *Carbon*, 2013, **53**, 321–326.
61 J.-H. Lee, E. K. Lee, W.-J. Joo, Y. Jang, B.-S. Kim, J. Y. Lim, S.-H. Choi, S. J. Ahn, J. R. Ahn, M.-H. Park, C.-W. Yang, B. L. Choi, S.-W. Hwang and D. Whang, *Science*, 2014, **344**, 286–289.
62 G. Wang, M. Zhang, Y. Zhu, G. Ding, D. Jiang, Q. Guo, S. Liu, X. Xie, P. K. Chu, Z. Di and X. Wang, *Sci. Rep.*, 2013, **3**, 2465.
63 Y. Wu, G. Yu, H. Wang, B. Wang, Z. Chen, Y. Zhang, B. Wang, X. Shi, X. Xie, Z. Jin and X. Liu, *Carbon*, 2012, **50**, 5226–5231.
64 Z. Zou, L. Fu, X. Song, Y. Zhang and Z. Liu, *Nano Lett.*, 2014, **14**, 3832–3839.
65 M. Zeng, L. Tan, J. Wang, L. Chen, M. H. Rümmeli and L. Fu, *Chem. Mater.*, 2014, **26**, 3637–3643.
66 Y. Wu, H. Chou, H. Ji, Q. Wu, S. Chen, W. Jiang, Y. Hao, J. Kang, Y. Ren, R. D. Piner and R. S. Ruoff, *ACS Nano*, 2012, **6**, 7731–7738.
67 X. Liu, L. Fu, N. Liu, T. Gao, Y. Zhang, L. Liao and Z. Liu, *J. Phys. Chem. C*, 2011, **115**, 11976–11982.
68 T. Lin, F. Huang, D. Wan, H. Bi, X. Xie and M. Jiang, *Nanoscale*, 2013, **5**, 5847–5853.
69 H.-A. S. Shin, J. Ryu, S.-P. Cho, E.-K. Lee, S. Cho, C. Lee, Y.-C. Joo and B. H. Hong, *Phys. Chem. Chem. Phys.*, 2014, **16**, 3087–3094.
70 M. H. Rümmeli, M. Zeng, S. Melkhanova, S. Gorantla, A. Bachmatiuk, L. Fu, C. Yan, S. Oswald, R. G. Mendes, D. Makarov, O. Schmidt and J. Eckert, *Chem. Mater.*, 2013, **25**, 3880–3887.
71 G. Wang, D. Chen, Z. Lu, Q. Guo, L. Ye, X. Wei, G. Ding, M. Zhang, Z. Di and S. Liu, *Appl. Phys. Lett.*, 2014, **104**, 062103.
72 R. S. Weatherup, B. C. Bayer, R. Blume, C. Ducati, C. Baehtz, R. Schlögl and S. Hofmann, *Nano Lett.*, 2011, **11**, 4154–4160.
73 C. Mattevi, H. Kim and M. Chhowalla, *J. Mater. Chem.*, 2011, **21**, 3324–3334.
74 X. Li, C. W. Magnuson, A. Venugopal, R. M. Tromp, J. B. Hannon, E. M. Vogel, L. Colombo and R. S. Ruoff, *J. Am. Chem. Soc.*, 2011, **133**, 2816–2819.
75 H. Wang, G. Wang, P. Bao, S. Yang, W. Zhu, X. Xie and W.-J. Zhang, *J. Am. Chem. Soc.*, 2012, **134**, 3627–3630.
76 Z. Yan, J. Lin, Z. Peng, Z. Sun, Y. Zhu, L. Li, C. Xiang, E. L. Samuel, C. Kittrell and J. M. Tour, *ACS Nano*, 2012, **6**, 9110–9117.

77 H. Zhou, W. J. Yu, L. Liu, R. Cheng, Y. Chen, X. Huang, Y. Liu, Y. Wang, Y. Huang and X. Duan, *Nat. Commun.*, 2013, **4**, 2096.
78 Y. Hao, M. S. Bharathi, L. Wang, Y. Liu, H. Chen, S. Nie, X. Wang, H. Chou, C. Tan, B. Fallahazad, H. Ramanarayan, C. W. Magnuson, E. Tutuc, B. I. Yakobson, K. F. McCarty, Y.-W. Zhang, P. Kim, J. Hone, L. Colombo and R. S. Ruoff, *Science*, 2013, **342**, 720–723.
79 S. Bae, H. Kim, Y. Lee, X. Xu, J.-S. Park, Y. Zheng, J. Balakrishnan, T. Lei, H. Ri Kim, Y. I. Song, Y.-J. Kim, K. S. Kim, B. Ozyilmaz, J.-H. Ahn, B. H. Hong and S. Iijima, *Nat. Nanotechnol.*, 2010, **5**, 574–578.
80 G. H. Han, H.-J. Shin, E. S. Kim, S. J. Chae, J.-Y. Choi and Y. H. Lee, *Nano*, 2011, **6**, 59–65.
81 J. Xue, J. Sanchez-Yamagishi, D. Bulmash, P. Jacquod, A. Deshpande, K. Watanabe, T. Taniguchi, P. Jarillo-Herrero and B. J. LeRoy, *Nat. Mater.*, 2011, **10**, 282–285.
82 W. Gannett, W. Regan, K. Watanabe, T. Taniguchi, M. F. Crommie and A. Zettl, *Appl. Phys. Lett.*, 2011, **98**, 242105.
83 L. Song, L. Ci, H. Lu, P. B. Sorokin, C. Jin, J. Ni, A. G. Kvashnin, D. G. Kvashnin, J. Lou, B. I. Yakobson and P. M. Ajayan, *Nano Lett.*, 2010, **10**, 3209–3215.
84 G. R. Whittell and I. Manners, *Angew. Chem., Int. Ed.*, 2011, **50**, 10288–10289.
85 Y. Shi, C. Hamsen, X. Jia, K. K. Kim, A. Reina, M. Hofmann, A. L. Hsu, K. Zhang, H. Li, Z.-Y. Juang, M. S. Dresselhaus, L.-J. Li and J. Kong, *Nano Lett.*, 2010, **10**, 4134–4139.
86 G. Constant and R. Feurer, *J. Less-Common Met.*, 1981, **82**, 113–118.
87 K. K. Kim, A. Hsu, X. Jia, S. M. Kim, Y. Shi, M. Hofmann, D. Nezich, J. F. Rodriguez-Nieva, M. Dresselhaus, T. Palacios and J. Kong, *Nano Lett.*, 2012, **12**, 161–166.
88 H. Jaehyun, L. Jun-Young, K. Heemin and Y. Jong-Souk, *Nanotechnology*, 2014, **25**, 145604.
89 G. Kim, A. R. Jang, H. Y. Jeong, Z. Lee, D. J. Kang and H. S. Shin, *Nano Lett.*, 2013, **13**, 1834–1839.
90 L. Wang, B. Wu, J. Chen, H. Liu, P. Hu and Y. Liu, *Adv. Mater.*, 2014, **26**, 1559–1564.
91 R. Y. Tay, M. H. Griep, G. Mallick, S. H. Tsang, R. S. Singh, T. Tumlin, E. H. T. Teo and S. P. Karna, *Nano Lett.*, 2014, **14**, 839–846.
92 Y. Yu, C. Li, Y. Liu, L. Su, Y. Zhang and L. Cao, *Sci. Rep.*, 2013, **3**, 1866.
93 A. M. van der Zande, P. Y. Huang, D. A. Chenet, T. C. Berkelbach, Y. You, G.-H. Lee, T. F. Heinz, D. R. Reichman, D. A. Muller and J. C. Hone, *Nat. Mater.*, 2013, **12**, 554–561.
94 J. Zhang, H. Yu, W. Chen, X. Tian, D. Liu, M. Cheng, G. Xie, W. Yang, R. Yang, X. Bai, D. Shi and G. Zhang, *ACS Nano*, 2014, **8**, 6024–6030.
95 A. L. Elías, N. Perea-López, A. Castro-Beltrán, A. Berkdemir, R. Lv, S. Feng, A. D. Long, T. Hayashi, Y. A. Kim, M. Endo, H. R. Gutiérrez, N. R. Pradhan, L. Balicas, T. E. Mallouk, F. López-Urías, H. Terrones and M. Terrones, *ACS Nano*, 2013, **7**, 5235–5242.
96 C. Cong, J. Shang, X. Wu, B. Cao, N. Peimyoo, C. Qiu, L. Sun and T. Yu, *Adv. Opt. Mater.*, 2013, **2**, 131–136.
97 Y. Zhang, Y. Zhang, Q. Ji, J. Ju, H. Yuan, J. Shi, T. Gao, D. Ma, M. Liu, Y. Chen, X. Song, H. Y. Hwang, Y. Cui and Z. Liu, *ACS Nano*, 2013, **7**, 8963–8971.
98 G. W. Shim, K. Yoo, S.-B. Seo, J. Shin, D. Y. Jung, I.-S. Kang, C. W. Ahn, B. J. Cho and S.-Y. Choi, *ACS Nano*, 2014, **8**, 6655–6662.
99 X. Wang, Y. Gong, G. Shi, W. L. Chow, K. Keyshar, G. Ye, R. Vajtai, J. Lou, Z. Liu, E. Ringe, B. K. Tay and P. M. Ajayan, *ACS Nano*, 2014, **8**, 5125–5131.
100 J.-K. Huang, J. Pu, C.-L. Hsu, M.-H. Chiu, Z.-Y. Juang, Y.-H. Chang, W.-H. Chang, Y. Iwasa, T. Takenobu and L.-J. Li, *ACS Nano*, 2013, **8**, 923–930.
101 J. A. Wilson and A. D. Yoffe, *Adv. Phys.*, 1969, **18**, 193–335.
102 C. Ataca, H. Şahin and S. Ciraci, *J. Phys. Chem. C*, 2012, **116**, 8983–8999.
103 X. Huang, Z. Zeng and H. Zhang, *Chem. Soc. Rev.*, 2013, **42**, 1934–1946.
104 B. Radisavljevic, A. Radenovic, J. Brivio, V. Giacometti and A. Kis, *Nat. Nanotechnol.*, 2011, **6**, 147–150.
105 Y. Zhan, Z. Liu, S. Najmaei, P. M. Ajayan and J. Lou, *Small*, 2012, **8**, 966–971.
106 Y.-H. Lee, X.-Q. Zhang, W. Zhang, M.-T. Chang, C.-T. Lin, K.-D. Chang, Y.-C. Yu, J. T.-W. Wang, C.-S. Chang, L.-J. Li and T.-W. Lin, *Adv. Mater.*, 2012, **24**, 2320–2325.
107 X. Wang, H. Feng, Y. Wu and L. Jiao, *J. Am. Chem. Soc.*, 2013, **135**, 5304–5307.
108 Q. Ji, Y. Zhang, T. Gao, Y. Zhang, D. Ma, M. Liu, Y. Chen, X. Qiao, P.-H. Tan, M. Kan, J. Feng, Q. Sun and Z. Liu, *Nano Lett.*, 2013, **13**, 3870–3877.
109 X. Ling, Y.-H. Lee, Y. Lin, W. Fang, L. Yu, M. S. Dresselhaus and J. Kong, *Nano Lett.*, 2014, **14**, 464–472.
110 Y.-H. Lee, L. Yu, H. Wang, W. Fang, X. Ling, Y. Shi, C.-T. Lin, J.-K. Huang, M.-T. Chang, C.-S. Chang, M. Dresselhaus, T. Palacios, L.-J. Li and J. Kong, *Nano Lett.*, 2013, **13**, 1852–1857.
111 H. R. Gutierrez, N. Perea-Lopez, A. L. Elias, A. Berkdemir, B. Wang, R. Lv, F. Lopez-Urias, V. H. Crespi, H. Terrones and M. Terrones, *Nano Lett.*, 2013, **13**, 3447–3454.
112 J. Shaw, H. Zhou, Y. Chen, N. Weiss, Y. Liu, Y. Huang and X. Duan, *Nano Res.*, 2014, **7**, 1–7.
113 X. Fan, Z. Shen, A. Q. Liu and J.-L. Kuo, *Nanoscale*, 2012, **4**, 2157–2165.
114 C.-K. Chang, S. Kataria, C.-C. Kuo, A. Ganguly, B.-Y. Wang, J.-Y. Hwang, K.-J. Huang, W.-H. Yang, S.-B. Wang, C.-H. Chuang, M. Chen, C.-I. Huang, W.-F. Pong, K.-J. Song, S.-J. Chang, J.-H. Guo, Y. Tai, M. Tsujimoto, S. Isoda, C.-W. Chen, L.-C. Chen and K.-H. Chen, *ACS Nano*, 2013, **7**, 1333–1341.
115 B. Muchharla, A. Pathak, Z. Liu, L. Song, T. Jayasekera, S. Kar, R. Vajtai, L. Balicas, P. M. Ajayan, S. Talapatra and N. Ali, *Nano Lett.*, 2013, **13**, 3476–3481.

116 G. Fiori, A. Betti, S. Bruzzone and G. Iannaccone, *ACS Nano*, 2012, **6**, 2642–2648.
117 M. P. Levendorf, C.-J. Kim, L. Brown, P. Y. Huang, R. W. Havener, D. A. Muller and J. Park, *Nature*, 2012, **488**, 627–632.
118 Z. Liu, L. Ma, G. Shi, W. Zhou, Y. Gong, S. Lei, X. Yang, J. Zhang, J. Yu, K. P. Hackenberg, A. Babakhani, J.-C. Idrobo, R. Vajtai, J. Lou and P. M. Ajayan, *Nat. Nanotechnol.*, 2013, **8**, 119–124.
119 Y. Gao, Y. Zhang, P. Chen, Y. Li, M. Liu, T. Gao, D. Ma, Y. Chen, Z. Cheng, X. Qiu, W. Duan and Z. Liu, *Nano Lett.*, 2013, **13**, 3439–3443.
120 G. H. Han, J. A. Rodríguez-Manzo, C.-W. Lee, N. J. Kybert, M. B. Lerner, Z. J. Qi, E. N. Dattoli, A. M. Rappe, M. Drndic and A. T. C. Johnson, *ACS Nano*, 2013, **7**, 10129–10138.
121 L. Liu, J. Park, D. A. Siegel, K. F. McCarty, K. W. Clark, W. Deng, L. Basile, J. C. Idrobo, A.-P. Li and G. Gu, *Science*, 2014, **343**, 163–167.
122 M. Yasumitsu, M. Eriko, K. Keiichi, K. Ryo, S. Yuki, S. Shoji and S. Hisanori, *Appl. Phys. Express*, 2012, **5**, 085102.
123 L. Ci, L. Song, C. Jin, D. Jariwala, D. Wu, Y. Li, A. Srivastava, Z. F. Wang, K. Storr, L. Balicas, F. Liu and P. M. Ajayan, *Nat. Mater.*, 2010, **9**, 430–435.
124 L. Liu and Z. Shen, *Appl. Phys. Lett.*, 2009, **95**, 252104.
125 Y. Liu, S. Bhowmick and B. I. Yakobson, *Nano Lett.*, 2011, **11**, 3113–3116.
126 Y. Gong, G. Shi, Z. Zhang, W. Zhou, J. Jung, W. Gao, L. Ma, Y. Yang, S. Yang, G. You, R. Vajtai, Q. Xu, A. H. MacDonald, B. I. Yakobson, J. Lou, Z. Liu and P. M. Ajayan, *Nat. Commun.*, 2014, **5**, 3193.
127 H. Lung-Hwa and C. Kai, *IEEE Trans. Microwave Theory Tech.*, 2002, **50**, 453–460.
128 C. Choon Sik, J. W. Lee and K. Jaeheung, *IEEE Trans. Microwave Theory Tech.*, 2006, **54**, 3968–3974.
129 P. Sutter, R. Cortes, J. Lahiri and E. Sutter, *Nano Lett.*, 2012, **12**, 4869–4874.
130 C. Huang, S. Wu, A. M. Sanchez, J. J. Peters, R. Beanland, J. S. Ross, P. Rivera, W. Yao, D. H. Cobden and X. Xu, arXiv preprint arXiv:1406.3122, 2014.
131 A. S. Mayorov, R. V. Gorbachev, S. V. Morozov, L. Britnell, R. Jalil, L. A. Ponomarenko, P. Blake, K. S. Novoselov, K. Watanabe, T. Taniguchi and A. K. Geim, *Nano Lett.*, 2011, **11**, 2396–2399.
132 P. J. Zomer, S. P. Dash, N. Tombros and B. J. van Wees, *Appl. Phys. Lett.*, 2011, **99**, 232104.
133 P. Zomer, M. Guimarães, J. Brant, N. Tombros and B. van Wees, arXiv preprint arXiv:1403.0399, 2014.
134 G.-H. Lee, Y.-J. Yu, X. Cui, N. Petrone, C.-H. Lee, M. S. Choi, D.-Y. Lee, C. Lee, W. J. Yoo, K. Watanabe, T. Taniguchi, C. Nuckolls, P. Kim and J. Hone, *ACS Nano*, 2013, **7**, 7931–7936.
135 R. g. Decker, Y. Wang, V. W. Brar, W. Regan, H.-Z. Tsai, Q. Wu, W. Gannett, A. Zettl and M. F. Crommie, *Nano Lett.*, 2011, **11**, 2291–2295.
136 S. J. Haigh, A. Gholinia, R. Jalil, S. Romani, L. Britnell, D. C. Elias, K. S. Novoselov, L. A. Ponomarenko, A. K. Geim and R. Gorbachev, *Nat. Mater.*, 2012, **11**, 764–767.
137 Y.-C. Lin, N. Lu, N. Perea-Lopez, J. Li, Z. Lin, X. Peng, C. H. Lee, C. Sun, L. Calderin, P. N. Browning, M. S. Bresnehan, M. J. Kim, T. S. Mayer, M. Terrones and J. A. Robinson, *ACS Nano*, 2014, **8**, 3715–3723.
138 L. Yu, Y.-H. Lee, X. Ling, E. J. G. Santos, Y. C. Shin, Y. Lin, M. Dubey, E. Kaxiras, J. Kong, H. Wang and T. Palacios, *Nano Lett.*, 2014, **14**, 3055–3063.
139 W. Zhang, C.-P. Chuu, J.-K. Huang, C.-H. Chen, M.-L. Tsai, Y.-H. Chang, C.-T. Liang, Y.-Z. Chen, Y.-L. Chueh, J.-H. He, M.-Y. Chou and L.-J. Li, *Sci. Rep.*, 2014, **4**, 3826.
140 Z. Liu, L. Song, S. Zhao, J. Huang, L. Ma, J. Zhang, J. Lou and P. M. Ajayan, *Nano Lett.*, 2011, **11**, 2032–2037.
141 W. Yang, G. Chen, Z. Shi, C.-C. Liu, L. Zhang, G. Xie, M. Cheng, D. Wang, R. Yang, D. Shi, K. Watanabe, T. Taniguchi, Y. Yao, Y. Zhang and G. Zhang, *Nat. Mater.*, 2013, **12**, 792–797.
142 J. M. Garcia, U. Wurstbauer, A. Levy, L. N. Pfeiffer, A. Pinczuk, A. S. Plaut, L. Wang, C. R. Dean, R. Buizza, A. M. Van Der Zande, J. Hone, K. Watanabe and T. Taniguchi, *Solid State Commun.*, 2012, **152**, 975–978.
143 P. Sutter, J. Lahiri, P. Zahl, B. Wang and E. Sutter, *Nano Lett.*, 2012, **13**, 276–281.
144 G. Gao, W. Gao, E. Cannuccia, J. Taha-Tijerina, L. Balicas, A. Mathkar, T. N. Narayanan, Z. Liu, B. K. Gupta, J. Peng, Y. Yin, A. Rubio and P. M. Ajayan, *Nano Lett.*, 2012, **12**, 3518–3525.
145 Z. Yan, Z. Peng, Z. Sun, J. Yao, Y. Zhu, Z. Liu, P. M. Ajayan and J. M. Tour, *ACS Nano*, 2011, **5**, 8187–8192.
146 M. Son, H. Lim, M. Hong and H. C. Choi, *Nanoscale*, 2011, **3**, 3089–3093.
147 M. Wang, S. K. Jang, W.-J. Jang, M. Kim, S.-Y. Park, S.-W. Kim, S.-J. Kahng, J.-Y. Choi, R. S. Ruoff, Y. J. Song and S. Lee, *Adv. Mater.*, 2013, **25**, 2746–2752.
148 S. Roth, F. Matsui, T. Greber and J. Osterwalder, *Nano Lett.*, 2013, **13**, 2668–2675.
149 T. Shujie, D. Guqiao, X. Xiaoming, C. Ji, W. Chen, D. Xuli, H. Fuqiang, L. Wei and J. Mianheng, *Carbon*, 2012, **50**, 329–331.
150 S. Tang, H. Wang, Y. Zhang, A. Li, H. Xie, X. Liu, L. Liu, T. Li, F. Huang, X. Xie and M. Jiang, *Sci. Rep.*, 2013, **3**, 2666.
151 S. M. Kim, A. Hsu, P. T. Araujo, Y.-H. Lee, T. Palacios, M. Dresselhaus, J.-C. Idrobo, K. K. Kim and J. Kong, *Nano Lett.*, 2013, **13**, 933–941.
152 T. Lin, Y. Wang, H. Bi, D. Wan, F. Huang, X. Xie and M. Jiang, *J. Mater. Chem.*, 2012, **22**, 2859–2862.
153 T. Lin, Z. Liu, M. Zhou, H. Bi, K. Zhang, F. Huang, D. Wan and Y. Zhong, *ACS Appl. Mater. Interfaces*, 2014, **6**, 3088–3092.
154 J. R. Wallbank, A. A. Patel, M. Mucha-Kruczyński, A. K. Geim and V. I. Fal'ko, *Phys. Rev. B: Condens. Matter*, 2013, **87**, 245408.

155 G. Giovannetti, P. A. Khomyakov, G. Brocks, P. J. Kelly and J. van den Brink, *Phys. Rev. B: Condens. Matter*, 2007, **76**, 073103.
156 J. Slawinska, I. Zasada and Z. Klusek, *Phys. Rev. B: Condens. Matter*, 2010, **81**, 155433.
157 J. Sławińska, I. Zasada, P. Kosiński and Z. Klusek, *Phys. Rev. B: Condens. Matter*, 2010, **82**, 085431.
158 R. Quhe, J. Zheng, G. Luo, Q. Liu, R. Qin, J. Zhou, D. Yu, S. Nagase, W.-N. Mei, Z. Gao and J. Lu, *NPG Asia Mater.*, 2012, **4**, e6.
159 A. Ramasubramaniam, D. Naveh and E. Towe, *Nano Lett.*, 2011, **11**, 1070–1075.
160 X. Zhong, R. G. Amorim, R. H. Scheicher, R. Pandey and S. P. Karna, *Nanoscale*, 2012, **4**, 5490–5498.
161 Z. Xiaoyang, L. Linyang and Z. Mingwen, *J. Phys.: Condens. Matter*, 2014, **26**, 095002.
162 Y. Sakai, T. Koretsune and S. Saito, *Phys. Rev. B: Condens. Matter*, 2011, **83**, 205434.
163 Y. Sakai, S. Saito and M. L. Cohen, *Phys. Rev. B: Condens. Matter*, 2014, **89**, 115424.
164 Y. Sakai and S. Saito, *J. Phys. Soc. Jpn.*, 2012, **81**, 103701.
165 H. Terrones, F. López-Urías and M. Terrones, *Sci. Rep.*, 2013, **3**, 1549.
166 K. Kośmider and J. Fernández-Rossier, *Phys. Rev. B: Condens. Matter*, 2013, **87**, 075451.
167 J. Kang, J. Li, S.-S. Li, J.-B. Xia and L.-W. Wang, *Nano Lett.*, 2013, **13**, 5485–5490.
168 J. He, K. Hummer and C. Franchini, *Phys. Rev. B: Condens. Matter*, 2014, **89**, 075409.
169 N. Lu, H. Guo, L. Li, J. Dai, L. Wang, W.-N. Mei, X. Wu and X. C. Zeng, *Nanoscale*, 2014, **6**, 2879–2886.
170 J. Kang, S. Tongay, J. Zhou, J. Li and J. Wu, *Appl. Phys. Lett.*, 2013, **102**, 012111.
171 A. Koma, K. Sunouchi and T. Miyajima, *J. Vac. Sci. Technol., B*, 1985, **3**, 724–724.
172 H. Fang, C. Battaglia, C. Carraro, S. Nemsak, B. Ozdol, J. S. Kang, H. A. Bechtel, S. B. Desai, F. Kronast, A. A. Unal, G. Conti, C. Conlon, G. K. Palsson, M. C. Martin, A. M. Minor, C. S. Fadley, E. Yablonovitch, R. Maboudian and A. Javey, *Proc. Natl. Acad. Sci. U. S. A.*, 2014, **111**, 6198–6202.
173 S. Tongay, W. Fan, J. Kang, J. Park, U. Koldemir, J. Suh, D. S. Narang, K. Liu, J. Ji, J. Li, R. Sinclair and J. Wu, *Nano Lett.*, 2014, **14**, 3185–3190.
174 Y. Yu, S. Hu, L. Su, L. Huang, Y. Liu, Z. Jin, A. A. Purezky, D. B. Geohegan, K. W. Kim and Y. Zhang, arXiv preprint arXiv:1403.6181, 2014.
175 W. J. Yu, Y. Liu, H. Zhou, A. Yin, Z. Li, Y. Huang and X. Duan, *Nat. Nanotechnol.*, 2013, **8**, 952–958.
176 W. Fu, F.-H. Du, J. Su, X.-H. Li, X. Wei, T.-N. Ye, K.-X. Wang and J.-S. Chen, *Sci. Rep.*, 2014, **4**, 4673.
177 Y. Shi, W. Zhou, A.-Y. Lu, W. Fang, Y.-H. Lee, A. L. Hsu, S. M. Kim, K. K. Kim, H. Y. Yang, L.-J. Li, J.-C. Idrobo and J. Kong, *Nano Lett.*, 2012, **12**, 2784–2791.
178 W. Dang, H. Peng, H. Li, P. Wang and Z. Liu, *Nano Lett.*, 2010, **10**, 2870–2876.
179 P. Gehring, B. F. Gao, M. Burghard and K. Kern, *Nano Lett.*, 2012, **12**, 5137–5142.
180 X. Zhang, F. Meng, J. R. Christianson, C. Arroyo-Torres, M. A. Lukowski, D. Liang, J. R. Schmidt and S. Jin, *Nano Lett.*, 2014, **14**, 3047–3054.
181 E. Hiroyuki, K. Takanori, K. Masayuki, T. Yoshiki and S. Kazuko, *Jpn. J. Appl. Phys.*, 2004, **43**, L123.
182 K. Ueno, K. Saiki, T. Shimada and A. Koma, *J. Vac. Sci. Technol., A*, 1990, **8**, 68–72.
183 H. Li, J. Cao, W. Zheng, Y. Chen, D. Wu, W. Dang, K. Wang, H. Peng and Z. Liu, *J. Am. Chem. Soc.*, 2012, **134**, 6132–6135.
184 Q. Wang, M. Safdar, K. Xu, M. Mirza, Z. Wang and J. He, *ACS Nano*, 2014, **8**, 7497–7505.
185 B. Aufray, A. Kara, S. Vizzini, H. Oughaddou, C. Leandri, B. Ealet and G. L. Lay, *Appl. Phys. Lett.*, 2010, **96**, 183102.
186 B. Lalmi, H. Oughaddou, H. Enriquez, A. Kara, S. Vizzini, B. Ealet and B. Aufray, *Appl. Phys. Lett.*, 2010, **97**, 223109.
187 A. Fleurence, R. Friedlein, T. Ozaki, H. Kawai, Y. Wang and Y. Yamada-Takamura, *Phys. Rev. Lett.*, 2012, **108**, 245501.
188 L. Meng, Y. Wang, L. Zhang, S. Du, R. Wu, L. Li, Y. Zhang, G. Li, H. Zhou, W. A. Hofer and H.-J. Gao, *Nano Lett.*, 2013, **13**, 685–690.
189 L. Li, Y. Yu, G. J. Ye, Q. Ge, X. Ou, H. Wu, D. Feng, X. H. Chen and Y. Zhang, *Nat. Nanotechnol.*, 2014, **9**, 372–377.
190 H. Liu, A. T. Neal, Z. Zhu, Z. Luo, X. Xu, D. Tománek and P. D. Ye, *ACS Nano*, 2014, **8**, 4033–4041.
191 Y. Deng, Z. Luo, N. J. Conrad, H. Liu, Y. Gong, S. Najmaei, P. M. Ajayan, J. Lou, X. Xu and P. D. Ye, *ACS Nano*, 2014, **8**, 8292–8299.
192 D. Jariwala, V. K. Sangwan, L. J. Lauhon, T. J. Marks and M. C. Hersam, *ACS Nano*, 2014, **8**, 1102–1120.
193 F. Schwierz, *Nat. Nanotechnol.*, 2010, **5**, 487–496.
194 E. V. Castro, K. S. Novoselov, S. V. Morozov, N. M. R. Peres, J. M. B. L. dos Santos, J. Nilsson, F. Guinea, A. K. Geim and A. H. C. Neto, *Phys. Rev. Lett.*, 2007, **99**, 216802.
195 J. B. Oostinga, H. B. Heersche, X. L. Liu, A. F. Morpurgo and L. M. K. Vandersypen, *Nat. Mater.*, 2008, **7**, 151–157.
196 M. Y. Han, B. Özyilmaz, Y. Zhang and P. Kim, *Phys. Rev. Lett.*, 2007, **98**, 206805.
197 C. Stampfer, S. Fringes, J. Güttinger, F. Molitor, C. Volk, B. Terrés, J. Dauber, S. Engels, S. Schnez and A. Jacobsen, *Front. Phys.*, 2011, **6**, 271–293.
198 L. A. Ponomarenko, A. K. Geim, A. A. Zhukov, R. Jalil, S. V. Morozov, K. S. Novoselov, I. V. Grigorieva, E. H. Hill, V. V. Cheianov, V. I. Fal'ko, K. Watanabe, T. Taniguchi and R. V. Gorbachev, *Nat. Phys.*, 2011, **7**, 958–961.
199 W. J. Yu, Z. Li, H. Zhou, Y. Chen, Y. Wang, Y. Huang and X. Duan, *Nat. Mater.*, 2013, **12**, 246–252.
200 M. Sup Choi, G.-H. Lee, Y.-J. Yu, D.-Y. Lee, S. Hwan Lee, P. Kim, J. Hone and W. JongYoo, *Nat. Commun.*, 2013, **4**, 1624.
201 S. Bertolazzi, D. Krasnozhon and A. Kis, *ACS Nano*, 2013, **7**, 3246–3252.

202 K. F. Mak, C. Lee, J. Hone, J. Shan and T. F. Heinz, *Phys. Rev. Lett.*, 2010, **105**, 136805.
203 A. Splendiani, L. Sun, Y. Zhang, T. Li, J. Kim, C.-Y. Chim, G. Galli and F. Wang, *Nano Lett.*, 2010, **10**, 1271–1275.
204 O. Lopez-Sanchez, D. Lembke, M. Kayci, A. Radenovic and A. Kis, *Nat. Nanotechnol.*, 2013, **8**, 497–501.
205 Y. Ye, Z. Ye, M. Gharghi, H. Zhu, M. Zhao, Y. Wang, X. Yin and X. Zhang, *Appl. Phys. Lett.*, 2014, **104**, 193508.
206 R. Sundaram, M. Engel, A. Lombardo, R. Krupke, A. Ferrari, P. Avouris and M. Steiner, *Nano Lett.*, 2013, **13**, 1416–1421.
207 M. Fontana, T. Deppe, A. K. Boyd, M. Rinzan, A. Y. Liu, M. Paranjape and P. Barbara, *Sci. Rep.*, 2013, **3**, 1634.
208 G. Konstantatos, M. Badioli, L. Gaudreau, J. Osmond, M. Bernechea, F. P. G. de Arquer, F. Gatti and F. H. Koppens, *Nat. Nanotechnol.*, 2012, **7**, 363–368.
209 K. Roy, M. Padmanabhan, S. Goswami, T. P. Sai, G. Ramalingam, S. Raghavan and A. Ghosh, *Nat. Nanotechnol.*, 2013, **8**, 826–830.
210 C. O. Kim, S. Kim, D. H. Shin, S. S. Kang, J. M. Kim, C. W. Jang, S. S. Joo, J. S. Lee, J. H. Kim and S.-H. Choi, *Nat. Commun.*, 2014, **5**, 3249.
211 C.-H. Liu, Y.-C. Chang, T. B. Norris and Z. Zhong, *Nat. Nanotechnol.*, 2014, **9**, 273–278.
212 O. Lopez-Sanchez, E. Alarcon Llado, V. Koman, A. Fontcuberta i Morral, A. Radenovic and A. Kis, *ACS Nano*, 2014, **8**, 3042–3048.
213 D. Jariwala, V. K. Sangwan, C.-C. Wu, P. L. Prabhumirashi, M. L. Geier, T. J. Marks, L. J. Lauhon and M. C. Hersam, *Proc. Natl. Acad. Sci. U. S. A.*, 2013, **110**, 18076–18080.
214 R. Cheng, D. Li, H. Zhou, C. Wang, A. Yin, S. Jiang, Y. Liu, Y. Chen, Y. Huang and X. Duan, arXiv preprint arXiv:1403.3447, 2014.
215 C.-H. Lee, G.-H. Lee, A. M. van der Zande, W. Chen, Y. Li, M. Han, X. Cui, G. Arefe, C. Nuckolls and T. F. Heinz, arXiv preprint arXiv:1403.3062, 2014.
216 M. M. Furchi, A. Pospischil, F. Libisch, J. Burgdörfer and T. Mueller, arXiv preprint arXiv:1403.2652, 2014.
217 A. Pospischil, M. M. Furchi and T. Mueller, *Nat. Nanotechnol.*, 2014, **9**, 257–261.
218 Y. Zhang, J. Ye, Y. Matsuhashi and Y. Iwasa, *Nano Lett.*, 2012, **12**, 1136–1140.
219 B. W. H. Baugher, H. O. H. Churchill, Y. Yang and P. Jarillo-Herrero, *Nat. Nanotechnol.*, 2014, **9**, 262–267.
220 J. S. Ross, P. Klement, A. M. Jones, N. J. Ghimire, J. Yan, D. G. Mandrus, T. Taniguchi, K. Watanabe, K. Kitamura, W. Yao, D. H. Cobden and X. Xu, *Nat. Nanotechnol.*, 2014, **9**, 268–272.
221 K. F. Mak, K. He, J. Shan and T. F. Heinz, *Nat. Nanotechnol.*, 2012, **7**, 494–498.
222 H. Zeng, J. Dai, W. Yao, D. Xiao and X. Cui, *Nat. Nanotechnol.*, 2012, **7**, 490–493.

